



# Upscaling of nanoparticle transport in porous media under unfavorable conditions: Pore scale to Darcy scale



N. Seetha<sup>a</sup>, Amir Raof<sup>b</sup>, M.S. Mohan Kumar<sup>c,\*</sup>, S. Majid Hassanizadeh<sup>b</sup>

<sup>a</sup> Department of Civil Engineering, Indian Institute of Science, Bangalore 560012, India

<sup>b</sup> Department of Earth Sciences, Utrecht University, P.O. Box 80021, 3508 TA Utrecht, The Netherlands

<sup>c</sup> Department of Civil Engineering and Indo-French Cell for Water Sciences, Indian Institute of Science, Bangalore 560012, India

## ARTICLE INFO

### Article history:

Received 11 June 2016

Received in revised form 6 January 2017

Accepted 1 March 2017

Available online 6 March 2017

### Keywords:

Colloid transport

Nanoparticles

Deposition

Upscaling

Pore-network modeling

Darcy scale

## ABSTRACT

Transport and deposition of nanoparticles in porous media is a multi-scale problem governed by several pore-scale processes, and hence, it is critical to link the processes at pore scale to the Darcy-scale behavior. In this study, using pore network modeling, we develop correlation equations for deposition rate coefficients for nanoparticle transport under unfavorable conditions at the Darcy scale based on pore-scale mechanisms. The upscaling tool is a multi-directional pore-network model consisting of an interconnected network of pores with variable connectivities. Correlation equations describing the pore-averaged deposition rate coefficients under unfavorable conditions in a cylindrical pore, developed in our earlier studies, are employed for each pore element. Pore-network simulations are performed for a wide range of parameter values to obtain the breakthrough curves of nanoparticle concentration. The latter is fitted with macroscopic 1-D advection-dispersion equation with a two-site linear reversible deposition accounting for both equilibrium and kinetic sorption. This leads to the estimation of three Darcy-scale deposition coefficients: distribution coefficient, kinetic rate constant, and the fraction of equilibrium sites. The correlation equations for the Darcy-scale deposition coefficients, under unfavorable conditions, are provided as a function of measurable Darcy-scale parameters, including: porosity, mean pore throat radius, mean pore water velocity, nanoparticle radius, ionic strength, dielectric constant, viscosity, temperature, and surface potentials of the particle and grain surfaces. The correlation equations are found to be consistent with the available experimental results, and in qualitative agreement with Colloid Filtration Theory for all parameters, except for the mean pore water velocity and nanoparticle radius.

© 2016 Published by Elsevier B.V.

## 1. Introduction

Colloids are particles with size in the range between 10 nm to 10  $\mu\text{m}$ , and are ubiquitous in the subsurface (Bradford and Torkzaban, 2008; DeNovio et al., 2004). They exist in the subsurface in various forms such as bacteria, viruses, protozoa, humic substances, clays, mineral precipitates, engineered nanoparticles, etc. Prediction of nanoparticle deposition rates in porous media has several applications such as movement of pathogenic viruses and engineered nanoparticles in the subsurface, deep bed and river bank filtration for water treatment, and (bio)remediation of contaminants by engineered nanoparticles. Nanoparticle deposition in porous media is controlled by several factors such as the flow velocity (Li et al., 2008; Tong and Johnson, 2006; Zhang et al., 2013), grain size (Li et al., 2008; Shen et al., 2008), nanoparticle size (Sasidharan et al., 2014; Shen et al., 2008; Tong and Johnson, 2006), pH (Sadeghi et al., 2011), ionic strength (Sadeghi et al., 2011;

Sasidharan et al., 2014; Tufenkji and Elimelech, 2005), physical and chemical heterogeneity of grains and the particle surfaces (Li et al., 2008; Sasidharan et al., 2014; Schijven and Simunek, 2002; Shen et al., 2015; Tufenkji and Elimelech, 2005), temperature (Syngouna and Chrysikopoulos, 2010), and degree of saturation (Zhang et al., 2013). One expects complex mechanistic relationships between the deposition rate coefficients and the above-mentioned factors (Johnson et al., 2007a).

Because of their small size (<100 nm), nanoparticles may interact with the porous medium in a different way compared to the larger colloids, resulting in different retention mechanisms for nanoparticles and micron-sized particles. In contrast to the micrometer-sized particles, for which sedimentation and interception are the most dominant transport mechanisms, Brownian diffusion is the dominant transport mechanism for nanoparticles. Apart from this, the effect of the physical and chemical heterogeneity of the grain surface, and deposition in the primary minimum of the Derjaguin-Landau-Verwey-Overbeek (DLVO) energy profile (Derjaguin and Landau, 1941; Verwey and Overbeek, 1948) are more significant for nanoparticles as compared to micron-sized

\* Corresponding author.

E-mail address: [msmk@civil.iisc.ernet.in](mailto:msmk@civil.iisc.ernet.in) (M.S. Mohan Kumar).

particles due to their small size (Petosa et al., 2010). This emphasizes the need to study nanoparticles separately from larger, micrometer-sized colloids to better understand nanoparticle retention mechanisms.

Transport of nanoparticles in porous media spans over a wide range of length scales, from the sub-pore scale, where the particle-soil interaction forces determine the deposition, up to the Darcy scale, where the governing macroscopic equations of nanoparticle transport are formulated (Elimelech and O'Melia, 1990; Wood et al., 2004). Particle retention at the Darcy scale is due to the lumped effects of processes occurring at the pore scale. Therefore, by incorporating the pore-scale physics into the Darcy-scale model, we may upscale particle transport from pore to the Darcy scale. Colloid deposition rate in porous media under favorable conditions (i.e., in the absence of electrostatic repulsion between colloid and grain surface) can be predicted using Colloid Filtration Theory (CFT) for micron-sized particles (Li et al., 2005; Nelson and Ginn, 2011; Rajagopalan and Tien, 1976; Tufenkji and Elimelech, 2004), which provides a first-order irreversible kinetic model (Yao et al., 1971). In CFT, the particle removal is described using a single collector. It is assumed that a control volume in the continuum scale comprises a collection of identical collectors. Therefore, the upscaling is based on the assumption that the processes observed and equations developed at the microscale holds at the macroscale (Logan et al., 1995; Molnar et al., 2015; Nelson and Ginn, 2011). CFT expresses the attachment rate coefficient in terms of single collector contact efficiency,  $\eta_0$ , defined as the ratio of the rate at which colloids strike the collector surface to the rate at which particles flow toward the collector. Three individual retention mechanisms contribute to  $\eta_0$ : Brownian diffusion, interception, and sedimentation (Yao et al., 1971). Several correlation equations for  $\eta_0$  are available in the literature (e.g., Kamai et al., 2015; Long and Hilpert, 2009; Ma et al., 2013; Messina et al., 2015; Nelson and Ginn, 2011; Rajagopalan and Tien, 1976; Tufenkji and Elimelech, 2004; Yao et al., 1971), which differ in the domain geometries, range of parameter values, and physical mechanisms or forces considered in modeling transport of colloid to the collector surface (Molnar et al., 2015). The existing correlation equations have been found to overpredict particle deposition at low flow velocity conditions ( $\leq 10^{-6}$  m/s), which are typical of groundwater flow, and for nanoscale particles, leading to  $\eta_0$  values being larger than unity (Ma et al., 2013; Nelson and Ginn, 2011; Petosa et al., 2010). Instead of using the results from the mechanistic pore-scale models, Kamai et al. (2015) developed a new correlation equation for  $\eta_0$  under favorable conditions by using experimental data to parameterize mechanistically based  $\eta_0$  equation of Rajagopalan and Tien (1976). This is done to account for the physical processes and natural complexities (heterogeneities, incomplete mixing within and between pores, and particle-collector and particle-particle interactions such as aggregation and agglomeration) in realistic porous media, which were not included in the mechanistic microscopic model. Colloids and grain surfaces are usually negatively charged under the prevailing environmental conditions, which lead to repulsive force acting between them, making the conditions unfavorable for particle deposition (Johnson et al., 2007a, b; Molnar et al., 2015). Under unfavorable conditions, in order to account for the reduction in particle deposition, due to the presence of an energy barrier between the colloid and the grain surface, the expression for attachment rate coefficient based on CFT is multiplied by a factor  $\alpha$ , called attachment efficiency ( $\alpha < 1$ ) (Tufenkji and Elimelech, 2004). CFT assumes the attachment efficiency to be independent of system hydrodynamics and grain sizes. Nevertheless, experimental results indicate that attachment efficiency is affected by the flow velocity (Johnson et al., 2007b; Keller et al., 2004; Shen et al., 2010; Tong and Johnson, 2006; Zhang et al., 2015) as well as grain diameter (Ren et al., 2001; Shen et al., 2008). Although attachment efficiency can be calculated using the theoretical expressions derived based on DLVO theory of colloidal stability (Derjaguin and Landau, 1941; Verwey and Overbeek, 1948) (Shen et al., 2007, 2010; Spielman and Friedlander, 1974), a quantitative relationship between  $\alpha$  and various controlling factors (such as system chemistry, hydrodynamics, particle

size, and collector size) is not available yet. Bai and Tien (1999), Elimelech (1992), and Park et al. (2012) derived empirical expressions for  $\alpha$  in terms of various dimensionless physico-chemical parameters. However, the applicability of their formulation is restricted to the range of experimental conditions under which they are developed, and are incapable of revealing the underlying retention mechanisms (Ma et al., 2011). Chang and Chan (2008) developed a correlation equation for  $\alpha$  by using a triangular network model to represent the porous medium and adopting the Brownian dynamic simulation method to track colloidal particles moving through the network. The correlation equation was developed as the sum of contributions from four individual deposition mechanisms: Brownian diffusion, DLVO interactions, sedimentation, and interception (Chang and Chan, 2008). Mechanistic-based correlation equations to predict the colloid deposition rates under unfavorable conditions do not exist. Colloid deposition rate coefficients are often determined by fitting the colloid breakthrough curve (BTC), obtained from experiments, to the advection-dispersion-deposition models.

Pore-network modeling offers a valuable tool for investigating the macroscopic behavior by accounting for the relevant physics at the underlying pore scale. Using pore-network modeling, fluid flow and transport processes are simulated directly at the microscopic scale without assuming a-priori macroscopic equations. This is done by idealizing the pore spaces as an interconnected network of pore elements (i.e., pore bodies and pore throats) of different sizes which are variably connected to each other, and simulating flow and transport through the network of pores (Raouf, 2011). Details on pore-network modeling can be found in Raouf et al. (2013). Pore-network models have been widely used to study the adsorption of solutes (Raouf et al., 2010; Sugita et al., 1995), reactive solute transport and porosity evolution (Raouf et al., 2013), particle transport (Chang and Chan, 2008; Kim and Whittle, 2006; Lee and Koplik, 2001; Sharma and Yortsos, 1987), multiphase flow in porous media (Niasar et al., 2009, 2010; Raeesi and Piri, 2009; Valvatne et al., 2005), biofilm growth and permeability reduction (Qin and Hassanizadeh, 2015; Suchomel et al., 1998; Thullner et al., 2002), macroscopic dispersion (Acharya et al., 2007; Armatas, 2006; Bijeljic and Blunt, 2007; Bijeljic et al., 2004; Li et al., 2014; Vasilyev et al., 2012), reaction rates (Knutson et al., 2007; Li et al., 2006; Meile and Tuncay, 2006), and hydraulic conductivity (Thullner et al., 2002; Van Marcke et al., 2010; Vervoort and Cattle, 2003).

The objectives of this study are to upscale nanoparticle transport in porous media from pore scale to the Darcy scale using pore-network modeling, and to develop correlation equations for the Darcy-scale deposition rate coefficients under unfavorable conditions in terms of ten measurable parameters at Darcy scale, including porosity, mean pore water velocity, mean pore throat radius, nanoparticle radius, solution ionic strength, liquid viscosity, surface potentials of nanoparticles and grain surfaces, temperature, and solution dielectric constant. Applying pore scale parameters within the pore network modeling, we account for the effects of pore-scale deposition mechanisms, pore structure and pore connectivity on the deposition rate coefficients at the Darcy scale. Although physical and chemical heterogeneity of the soil affect nanoparticle retention under unfavorable conditions, here we assume that the grain surface is homogeneous in order to illustrate the effect of parameters such as porosity, mean pore water velocity, mean pore throat radius, nanoparticle radius, solution ionic strength, liquid viscosity, surface potentials of nanoparticles and grain surfaces, temperature, and solution dielectric constant on nanoparticle deposition under unfavorable conditions. We use PoreFlow, a three-dimensional multi-directional pore-network model developed by Raouf et al. (2010, 2013), which represents a porous medium as an interconnected network of pore throats and pore bodies with random pore connectivities to represent randomness of pore structures. The simulations are performed for a range of flow velocity values ( $10^{-8}$  to  $3 \times 10^{-6}$  m/s), representing groundwater flow velocities (Nelson and Ginn, 2011). We followed the approach of Raouf and Hassanizadeh (2010) and Raouf et al.

(2010) to upscale nanoparticle transport in porous media from pore to the Darcy scale. Raof and Hassanizadeh (2010) derived expressions for the effective attachment and detachment rate coefficients for a single tube, for solutes undergoing equilibrium adsorption at the surface of a cylindrical pore as a function of pore-scale parameters, such as the equilibrium distribution coefficient, pore radius, and solute diffusion coefficient. Next, the tube-scale relations were incorporated into a pore-network model to upscale solute transport to the Darcy scale, and to derive quantitative relationships between Darcy-scale adsorption parameters and the pore-scale flow and adsorption parameters (Raof et al., 2010). The sequence of steps that we have followed to develop the Darcy-scale correlation expressions for nanoparticles are:

- (1) Derive correlation equations for the average nanoparticle deposition rate coefficients in a cylindrical pore in terms of nine pore-scale parameters: the pore radius, nanoparticle radius, mean flow velocity, solution ionic strength, fluid viscosity, temperature, fluid dielectric constant, and nanoparticle and collector surface potentials (Seetha et al., 2015a).
- (2) Incorporate these pore-scale correlation equations in a multi-directional pore-network model (Raof et al., 2010) to simulate the transport of nanoparticles at Darcy scale for a range of values of measurable Darcy-scale parameters.
- (3) Average the resulting nanoparticle concentration at the outlet of the pore network to get the nanoparticle BTC.
- (4) Fit the resulting nanoparticle BTC against 1-D advection-dispersion-deposition equation, in order to determine the values of Darcy-scale deposition rate coefficients, and
- (5) Develop correlation equations for the Darcy-scale nanoparticle deposition rate coefficients by performing a multiple-linear regression analysis between the estimated Darcy-scale deposition rate coefficients and various measurable parameters.

## 2. Deposition rate coefficients of nanoparticles in a cylindrical pore

Seetha et al. (2015a) developed correlation equations for the pore-averaged deposition rate coefficients of nanoparticles in a cylindrical pore under unfavorable conditions as a function of several pore-scale parameters including: pore radius, nanoparticle radius, mean flow velocity, solution ionic strength, fluid viscosity, temperature, fluid dielectric constant, and nanoparticle and collector surface potentials, as briefly described below.

Seetha et al. (2015a) divided the pore space into three different regions, namely, bulk, diffusion, and potential regions, based on the dominant processes and forces acting within each region. Transport of nanoparticles in the cylindrical pore was simulated by solving the advection-diffusion equation in the bulk and diffusion regions, subject to a first-order reversible kinetic deposition at the pore wall. The expressions for the mass transfer rate coefficients between the pore and the wall regions were derived in terms of the interaction energy profile acting between the nanoparticle and the collector. Five dimensionless pore-scale parameters were formulated:  $N_{E1}$ ,  $N_{DL}$ ,  $Pe$ ,  $A$  and  $\lambda^*$ . Here  $N_{E1} = \frac{\pi \epsilon \epsilon_0 a (\psi_1^2 + \psi_2^2)}{k_B T}$  represents the sum of squares of surface potentials of nanoparticle and collector surfaces, where  $\psi_1$  and  $\psi_2$  are the surface potentials of the nanoparticle and collector, respectively,  $\epsilon$  is the dielectric constant of water,  $\epsilon_0$  is the permittivity of vacuum,  $a$  is the nanoparticle radius,  $k_B$  is the Boltzmann constant, and  $T$  is the absolute temperature. The dimensionless coefficient  $N_{DL} = \kappa a$  represents the ratio of nanoparticle radius to double layer thickness; where  $\kappa = \sqrt{2000 N_A e^2 / \epsilon \epsilon_0 k_B T}$  is the inverse Debye-Huckel length,  $N_A$  is Avogadro number,  $I$  is the solution ionic strength, and  $e$  is the elementary charge. The Péclet number,  $Pe = \frac{v_m R}{D_\infty}$  is defined as the ratio of the advective transport flux to the diffusive transport flux, where  $v_m$  is the mean flow velocity,  $R$  is the pore radius,  $D_\infty$  is the nanoparticle bulk diffusion coefficient given by Stoke-

Einstein relation as  $D_\infty = (k_B T / 6\pi \mu a)$ , and  $\mu$  is the dynamic viscosity of water. Finally,  $A = \frac{q}{R}$  is the interception parameter (ratio of nanoparticle radius to pore radius), and  $\lambda^* = \lambda/a$ , where  $\lambda$  is the characteristic wavelength of the interaction, usually taken as 100 nm. The pore-scale model results were used to obtain nanoparticle breakthrough concentration by averaging the concentration of mobile nanoparticles over a control volume within the pore. Similarly the average attached concentration was obtained by averaging the concentration of immobile nanoparticles over the surface of the pore within the control volume. The resulting BTCs and attached concentration curves obtained from the pore-scale model were fitted against a 1-D advection-dispersion equation with equilibrium or kinetic deposition model to obtain the values of pore-averaged deposition rate coefficients. In the case of an equilibrium model, we estimated  $K'_D = K_D/R$ , where  $K_D$  [L] is the equilibrium distribution coefficient at the pore wall. In the case of kinetic model,  $Da_{att}$  and  $Da_{det}$  were estimated, where  $Da_{att} = k_{att} R / v_m$  is the Damköhler number corresponding to the rate coefficient for nanoparticle attachment to the pore wall,  $Da_{det} = k_{det} R / v_m$  is the Damköhler number corresponding to the rate coefficient for nanoparticle detachment from the pore wall, and  $k_{att}$  [ $T^{-1}$ ] and  $k_{det}$  [ $T^{-1}$ ] are the average rate coefficients for nanoparticle attachment and detachment at pore scale. Seetha et al. (2015a) found that under unfavorable conditions, nanoparticle deposition at the pore scale is best described by an equilibrium model at low Péclet numbers (e.g.,  $Pe = 0.05$ ) and a kinetic model at high Péclet numbers (e.g.,  $Pe = 50$ ). There exists an intermediate range (around  $Pe = 5$ ), where both equilibrium and kinetic models can describe nanoparticle deposition. We derived correlation equations for the pore-scale nanoparticle deposition rate coefficients ( $K'_D$  or  $Da_{att}$  and  $Da_{det}$ ) under unfavorable conditions. This was done by performing a multiple-linear regression analysis between the estimated deposition rate coefficients ( $K'_D$  or  $Da_{att}$  and  $Da_{det}$ ) for a single pore and various pore-scale parameters ( $N_{E1}$ ,  $N_{DL}$ ,  $Pe$ ,  $A$  and  $\lambda^*$ ). We obtained:

$$K'_D = p_1 N_{E1}^{p_2} N_{DL}^{p_3} Pe^{p_4} A^{p_5} \lambda^{*p_6} \quad (1)$$

$$Da_{(att)} = q_1 N_{E1}^{q_2} N_{DL}^{q_3} Pe^{q_4} A^{q_5} \lambda^{*q_6} \quad (2a)$$

$$Da_{(det)} = r_1 N_{E1}^{r_2} N_{DL}^{r_3} Pe^{r_4} \exp(r_5 A) \lambda^{*r_6} \quad (2b)$$

Here,  $p_i$ ,  $q_i$ , and  $r_i$  ( $i = 1, 2, \dots, 6$ ) are coefficients in correlation equations for  $K'_D$ ,  $Da_{att}$  and  $Da_{det}$ , respectively.

Seetha et al. (2015a) classified nanoparticles into three groups: Group I ( $\lambda^* \geq 5$ ), Group II ( $2 \leq \lambda^* < 5$ ), and Group III ( $1 \leq \lambda^* < 2$ ). The estimated values of coefficients in Eqs. (1), (2a), (2b) for the three nanoparticle groups are given in Tables 4–6 of Seetha et al. (2015a). The pore-scale correlation equations were found to be consistent with the column-scale and pore-scale experimental results, and in qualitative agreement with CFT.

## 3. Pore network modeling

In this study, we use PoreFlow (Raof et al., 2013), which is a complex pore-network modeling tool capable of simulating fluid flow and multi-component reactive and adsorptive transport under saturated and variably saturated conditions. The porous medium is represented as a three-dimensional multi-directional pore-network model consisting of an interconnected network of spherical pore bodies and cylindrical pore throats (Raof et al., 2010). In order to mimic realistic porous media processes, network models should reproduce the main morphological and topological features (e.g., distribution of pore sizes and coordination number distribution, respectively) of real porous media. One of the main features of PoreFlow is that the pore throats can be oriented in several different directions, allowing a maximum pore coordination number of 26. Detailed information about the network generation is given in Raof and Hassanizadeh (2009). The radius

of the pore bodies is given by an uncorrelated truncated lognormal probability distribution. The radius of the pore throat is determined from the sizes of the two pore bodies it is connecting (Raouf and Hassanizadeh, 2009; Raouf et al., 2010). The equations governing the flow and transport through the network are given in Raouf et al. (2010), and are briefly described below.

### 3.1. Simulating flow through the network

Fluid flow through the network is simulated by imposing two different pressures at the inflow and outflow boundaries of the network. All other boundaries of the network parallel to the overall flow direction are considered as no-flow boundaries. Assuming laminar flow, the discharge  $q_{ij}$  through a given pore throat  $ij$  is described by Hagen-Poiseuille equation:

$$q_{ij} = \frac{\pi R_{ij}^4}{8\mu l} (P_j - P_i) \quad (3)$$

where  $R_{ij}$  is the radius of the pore throat,  $l$  is the length of the pore throat, and  $P_i$  and  $P_j$  are the pressures at pore bodies  $i$  and  $j$ , respectively. Under steady-state flow conditions, the sum of discharges of all pore throats connected to a pore body must be zero:

$$\sum_{j=1}^{z_i} q_{ij} = 0 \quad (4)$$

where  $z_i$  is the coordination number of the pore body  $i$  (which is between 2 and 26). Eq. (4) is valid for all pore bodies except for those at the inlet and outlet boundaries. Eqs. (3)–(4) are prescribed for all pore bodies and throats in the network, which results in a linear system of equations, with a sparse, symmetric and positive-definite coefficient matrix, to be solved for pore body pressures (Raouf et al., 2013). Then, the discharge through pore throats can be calculated using Eq. (3). Assuming the network to be a representative elementary volume, the average water velocity through the network,  $\bar{v}$  can then be calculated as (Raouf et al., 2013)

$$\bar{v} = \frac{Q}{\theta A_c} \quad (5)$$

where  $Q$  is the total discharge through the network which is the sum of fluxes through all pore throats at the inlet or outlet boundary of the network,  $\theta$  is the network porosity, and  $A_c$  is the cross-sectional area of the network perpendicular to the overall flow direction.

### 3.2. Simulating nanoparticle transport through the network

Following Raouf et al. (2010), we assume that the pore bodies and pore throats are completely mixed domains. This results in one (average) concentration being assigned to each pore body or pore throat. We consider only advective transport through pore bodies and neglect the nanoparticle deposition in the pore bodies. Hence, the governing equation for particle transport in a given pore body,  $i$ , can be written as:

$$V_i \frac{dc_i}{dt} = \sum_{j=1}^{N_{in}} q_{ij} c_{ij} - Q_i c_i \quad (6)$$

where  $V_i$  is the volume of the pore body  $i$ ,  $c_i$  is the average nanoparticle concentration in the pore body,  $c_{ij}$  is the average nanoparticle concentration in the pore throat  $ij$ ,  $Q_i$  is the total water flux leaving the pore body given as,  $Q_i = \sum_{j=1}^{N_{in}} q_{ij}$ , and  $N_{in}$  is the number of pore throats flowing into the pore body  $i$ .

For a pore throat, we consider advective transport only, but linear kinetic deposition is also taken into account. Thus, the governing equation

for nanoparticle transport in a pore throat is given as:

$$V_{ij} \frac{dc_{ij}}{dt} = q_{ij} c_j - q_{ij} c_{ij} - V_{ij} \alpha_{ij} (K_{d,ij} c_{ij} - s_{ij}) \quad (7)$$

where  $V_{ij}$  is the volume of the pore throat  $ij$ ,  $\alpha_{ij} [T^{-1}]$  is the first-order kinetic rate constant equal to the detachment rate coefficient,  $K_{d,ij} = \frac{k_{att,ij}}{\alpha_{ij}} [-]$  is the equilibrium distribution coefficient,  $k_{att,ij} [T^{-1}]$  is the attachment rate coefficient, and  $s_{ij}$  is the average attached concentration in the pore throat. The corresponding equation for the average attached concentration in a pore throat is given as

$$\frac{ds_{ij}}{dt} = \alpha_{ij} (K_{d,ij} c_{ij} - s_{ij}) \quad (8)$$

Seetha et al. (2015a) found that under unfavorable conditions, nanoparticle deposition in a cylindrical pore is best described by an equilibrium model at low Péclet numbers and by a kinetic model at high Péclet numbers. However, at an intermediate range, both equilibrium and kinetic models can describe nanoparticle deposition. Hence, at low Péclet numbers, nanoparticle deposition is described using an equilibrium model such that  $K_{d,ij} = \frac{2}{R_{ij}} K_{D,ij}$ , where  $K_{d,ij}$  is calculated for each throat  $ij$ , and  $K_{D,ij} = K'_{D,ij} R_{ij} [L]$  is a function of various dimensionless pore-scale parameters ( $N_{E1}$ ,  $N_{DL}$ ,  $Pe$ ,  $A$  and  $\lambda^*$ ) as given by Eq. (1). The attached concentration in the cylindrical pore is expressed in terms of number of attached particles/pore surface area and number of attached particles/pore volume in Seetha et al. (2015a) and Raouf et al. (2010), respectively. This resulted in the multiplication factor of  $2/R_{ij}$  in  $K_{D,ij}$  to define  $K_{d,ij}$ . To implement equilibrium adsorption, governing Eqs. (6)–(8) are solved by setting a very large value for  $\alpha_{ij}$ . At large Péclet numbers, where kinetic model prevails,  $K_{d,ij}$  can be calculated knowing  $k_{att,ij}$  and  $\alpha_{ij}$  as  $K_{d,ij} = \frac{k_{att,ij}}{\alpha_{ij}}$ , where  $k_{att,ij} = Da_{att,ij} v_{m,ij}/R_{ij}$  and  $\alpha_{ij} = Da_{det,ij} v_{m,ij}/R_{ij}$  are functions of various dimensionless pore-scale parameters ( $N_{E1}$ ,  $N_{DL}$ ,  $Pe$ ,  $A$  and  $\lambda^*$ ) as given by Eqs. (2a) and (2b), respectively.

The pore-scale correlation equations predict  $k_{att,ij} \ll \alpha_{ij}$  (Seetha et al., 2015a), which results in negligible deposition of nanoparticles. This is in contrast with some experimental results on nanoparticle retention under unfavorable conditions (Knappett et al., 2008; Li et al., 2008; Sasidharan et al., 2014; Shen et al., 2008; Tong and Johnson, 2006; Tufenkji and Elimelech, 2005). This implies that processes other than nanoparticle-collector interactions, such as, physical and chemical heterogeneity of both nanoparticle and the grain surface plays an important role in nanoparticle deposition under unfavorable conditions (Shen et al., 2011, 2015; Tong and Johnson, 2007; Torkzaban and Bradford, 2016; Trauscht et al., 2015). The pore-scale model developed by Seetha et al. (2015a) for a smooth and chemically homogeneous pore was very complex due to the combined effect of many pore-scale parameters and various forces (compiled into three different partial differential equations to be solved simultaneously for different locations across the pore) on nanoparticle deposition. Incorporating microscopic chemical and physical heterogeneity of the pore surface into the mathematical model would extremely complicate the model and the feasibility to perform modeling for a wide range of parameters. Moreover, there is a lack of sufficient information to model the physical and chemical heterogeneity of soil grain surfaces which would result in a large uncertainty in the parameter values and the obtained results. Hence, in this study while incorporating the pore-scale correlation equations developed by Seetha et al. (2015a) into the pore-network model, the effects of microscopic physical and chemical heterogeneity of the grain surface are accounted for by introducing a multiplier to  $K_D$  Eq. (1) and  $k_{att}$  Eq. (2a). We chose a value of 100 for the multiplier which also ensured that the ratio of attachment to detachment rate coefficients at the Darcy scale is approximately around 0.01, a value more realistic as observed from experimental data.

The governing Eqs. (6)–(8) when applied to all pores results in a linear system of equations, which are solved numerically using a fully implicit finite difference scheme (Raouf et al., 2010). Nanoparticle breakthrough concentration,  $\bar{c}$ , is obtained by averaging the concentration of pore bodies at the outflow boundary of the network. The concentrations of pore bodies are weighted by their discharges, resulting in a flux-averaged concentration, as given below.

$$\bar{c}(L, t) = \left[ \frac{\sum_i^{N_t} c_i(L, t) Q_i}{\sum_i^{N_t} Q_i} \right] \frac{1}{c_0} \quad (9)$$

where  $L$  is the network length,  $N_t$  denotes the number of pore bodies at the outlet boundary of the network, and  $c_0$  is the inlet nanoparticle concentration.

### 3.3. Parameters governing nanoparticle transport at Darcy scale

The six dimensionless parameters describing nanoparticle transport at Darcy scale are  $N_{E1}$ ,  $N_{DL}$ ,  $Pe_D$ ,  $A_{avg}$ ,  $\lambda^*$ , and  $\theta$ . The definitions and the physical interpretation of these dimensionless parameters are given in Table 1.

## 4. Modeling average (1-D) nanoparticle transport at Darcy scale

The nanoparticle transport at 1-D Darcy scale is described using advection-dispersion equation, with the deposition being described using a two-site model with terms accounting for both equilibrium and kinetic sorption Eqs. (10)–(11).

$$\frac{\partial \bar{c}}{\partial t} + \frac{\partial \bar{s}}{\partial t} = D_L \frac{\partial^2 \bar{c}}{\partial z^2} - \bar{v} \frac{\partial \bar{c}}{\partial z} \quad (10)$$

$$\bar{s} = \bar{s}_e + \bar{s}_k \quad (11)$$

where  $D_L$  is the dispersion coefficient at Darcy scale,  $\bar{s}$  is the average nanoparticle attached concentration, and  $\bar{s}_e$  and  $\bar{s}_k$  are the average attached concentrations at the equilibrium and kinetic sites, respectively. The nanoparticle deposition onto equilibrium and kinetic sites are assumed to be described by first-order models, and the corresponding governing equations are given in Eqs. (12)–(13), respectively.

$$\bar{s}_e = f K_{D(D)} \bar{c} \quad (12)$$

$$\frac{\partial \bar{s}_k}{\partial t} = \alpha_{(D)} [(1-f) K_{D(D)} \bar{c} - \bar{s}_k] \quad (13)$$

where  $K_{D(D)} = \frac{k_{att(D)}}{\alpha_{(D)}} [-]$  is the Darcy-scale equilibrium distribution coefficient,  $k_{att(D)} [T^{-1}]$  is the rate coefficient for nanoparticle attachment at Darcy scale,  $\alpha_{(D)} [T^{-1}]$  is the first-order kinetic rate constant equal to the detachment rate coefficient at Darcy scale, and  $f [-]$  is the fraction of sites assumed to be in equilibrium with the liquid phase. Substituting

Eqs. (11)–(13) into Eq. (10) leads to

$$\left(1 + f K_{D(D)}\right) \frac{\partial \bar{c}}{\partial t} = D_L \frac{\partial^2 \bar{c}}{\partial z^2} - \bar{v} \frac{\partial \bar{c}}{\partial z} - \alpha_{(D)} [(1-f) K_{D(D)} \bar{c} - \bar{s}_k] \quad (14)$$

Hence, the complete two-site model describing nanoparticle transport at 1-D Darcy scale is given by Eqs. (13)–(14).

The value of  $D_L$  is estimated by first simulating transport of a non-reactive tracer through the network, and then fitting the corresponding BTC obtained from the network with 1-D advection-dispersion model with no deposition. The values of the parameters describing nanoparticle deposition at Darcy scale, such as  $K_{D(D)}$ ,  $\alpha_{(D)}$ , and  $f$  are estimated by fitting the nanoparticle BTC obtained from the pore-network model (Section 3) against the 1-D advection-dispersion-deposition model i.e., Eqs. (13)–(14). The 1-D governing equations are solved numerically using an alternating three-step operator splitting approach, with the advection, dispersion and reaction operators being solved using explicit finite volume, fully implicit finite difference, and fourth-order Runge-Kutta methods, respectively (Seetha et al., 2015b).

Fig. 1 compares the nanoparticle BTC obtained from the pore-network model and the corresponding fitted curve with the 1-D model. It can be seen that the 1-D model accurately fits the BTC.

## 5. Correlation equations for nanoparticle deposition rate coefficients at Darcy scale

Pore-network model simulations are performed for a range of values of network parameters (Table 2), consistent with the range of values of pore-scale parameters for which the pore-scale correlation equations under unfavorable conditions were developed by Seetha et al. (2015a). All simulations are performed using a network of the size  $20 \times 20 \times 51$  pore bodies in the x, y and z directions (with z being the flow direction), and having a mean co-ordination number of 3.9, which represents a porous medium of sand type. The pore body radii are assumed to be lognormally distributed with a standard deviation of  $0.1 \bar{R}_{pb}$ , where  $\bar{R}_{pb}$  is the mean pore body radius. For all simulations, the average pore-water velocity through the network lies between  $10^{-7}$  and  $6 \times 10^{-6}$  m/s, which is consistent with the typical groundwater velocities in sandy aquifers. The pore-network model simulations are performed under unfavorable conditions for various combinations of network parameters, which resulted in a total of 600 simulations describing nanoparticle transport at the Darcy scale.

The estimated values of nanoparticle deposition parameters at Darcy scale ( $K_{D(D)}$ ,  $k_{att(D)}$ , and  $f$ ) obtained from the pore-network simulations formed the data set that was used to develop correlation equations for the Darcy-scale deposition coefficients ( $K_{D(D)}$ ,  $Da_{att(D)}$ , and  $f$ ) in terms

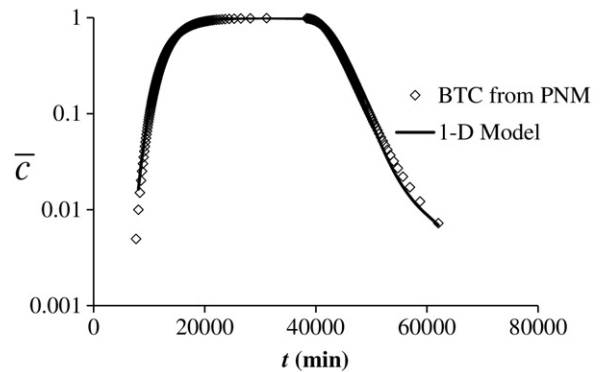


Fig. 1. Comparison of nanoparticle BTC obtained from the pore-network model (diamonds) and the 1-D Darcy-scale model (solid line) for  $N_{E1} = 10$ ,  $N_{DL} = 50$ ,  $Pe_D = 0.088$ ,  $A_{avg} = 0.00012$ ,  $\lambda^* = 10$ , and  $\theta = 0.392$ .

Table 1  
Darcy-scale parameters.

Parameter	Definition	Interpretation
$N_{E1}$	$\frac{\pi \epsilon_0 a (\psi_1^2 + \psi_2^2)}{k_B T}$	Represents the magnitudes of surface potentials
$N_{DL}$	$\kappa a$	Ratio of nanoparticle radius to double layer thickness
$Pe_D$	$\frac{\bar{v} \bar{R}}{D_m}$	Average network Péclet number, where $\bar{R}$ is the mean pore throat radius
$A_{avg}$	$a / \bar{R}$	Average interception parameter
$\lambda^*$	$\lambda / a$	Ratio of characteristic wavelength of interaction to the nanoparticle radius
$\theta$		Porosity

**Table 2**

Range of values of network parameters used in the simulations.

Parameter	Value
$N_{E1}$	10–400
$N_{DL}$	5.5–100
$Pe_D$	0.05–50
$A_{avg}$	0.00004–0.001
$\lambda^*$	1–10
$\theta$	0.3–0.5

of six dimensionless Darcy-scale parameters ( $N_{E1}$ ,  $N_{DL}$ ,  $Pe_D$ ,  $A_{avg}$ ,  $\lambda^*$ , and  $\theta$ ) as given in Eqs. (15)–(17), where  $Da_{att(D)} = \frac{k_{att(D)}\bar{R}}{v}$  [-] is the Damköhler number corresponding to the rate coefficient for nanoparticle attachment at the Darcy scale, and  $\bar{R}$  is the mean pore throat radius.

$$K_{D(D)} = a_1 N_{E1}^{a_2} N_{DL}^{a_3} Pe_D^{a_4} A_{avg}^{a_5} \lambda^{*a_6} \theta^{a_7} \quad (15)$$

$$Da_{att(D)} = b_1 N_{E1}^{b_2} N_{DL}^{b_3} Pe_D^{b_4} A_{avg}^{b_5} \lambda^{*b_6} \theta^{b_7} \quad (16)$$

$$f = \ln \left( c_1 N_{E1}^{c_2} N_{DL}^{c_3} Pe_D^{c_4} A_{avg}^{c_5} \lambda^{*c_6} \theta^{c_7} \right) \quad (17)$$

In Eqs. (15)–(17),  $a_i$ ,  $b_i$  and  $c_i$  ( $i = 1, 2, \dots, 7$ ) are constant parameters. The values of these constants are estimated by performing a multiple-linear regression analysis between the estimated nanoparticle deposition parameters at the Darcy scale and the six dimensionless Darcy-scale parameters. Eqs. (15)–(17) are formulated based on the assumption that the pore surface heterogeneity (or pore-scale multiplier) does not affect the values of the coefficients that appear in the power of different Darcy-scale parameters. To support this, we performed pore-network simulations with three different values of pore-scale multiplier: 1, 100, and 500. We observed that the trend between the estimated Darcy-scale deposition parameters ( $K_{D(D)}$ ,  $k_{att(D)}$ , and  $f$ ) vs the various Darcy-scale parameters, such as  $N_{E1}$ ,  $N_{DL}$ ,  $Pe_{avg}$ ,  $A_{avg}$  and  $\lambda^*$  remain unaltered irrespective of the value of the pore-scale multiplier, and the trend lines are parallel to each other in most of the cases. This indicates that the pore-scale multiplier has an effect only on the constant coefficient terms (i.e.,  $a_i$ ,  $b_i$  and  $c_i$ ) in the correlation equations for the Darcy-scale deposition rate coefficients (Eqs. 15–17). The results obtained in this study are based on applying a constant value of 100 for the multiplier in the pore-scale correlation equations Eqs. (1) and (2a).

Following the approach of Seetha et al. (2015a), we classified the nanoparticles into three groups based on their sizes: Group I ( $\lambda^* \geq 5$ ), Group II ( $2 \leq \lambda^* < 5$ ), and Group III ( $1 \leq \lambda^* < 2$ ). The estimated values of coefficients in Eqs. (15)–(17) for the three nanoparticle groups are given in Tables 3–5. Fig. 2 compares the estimated values of deposition parameters obtained from the pore-network model (by applying a multiplier of 100 in the pore-scale correlation equations) with the corresponding values predicted by the Darcy-scale correlation expressions (Eqs. (15)–(17)). It can be seen that there is a reasonable agreement between the calculated values and those predicted by the correlation equations. The predicted trends for the Darcy-scale deposition rate coefficients ( $K_{D(D)}$  and  $Da_{att(D)}$ ) vs the various Darcy-scale parameters ( $N_{E1}$ ,  $N_{DL}$ ,  $Pe_D$ ,  $A_{avg}$  and  $\lambda^*$ ) (Eqs. (15)–(17)) are consistent with the predicted trends for the pore-scale deposition rate coefficients ( $K'_D$  and  $Da_{att}$ ) vs the various pore-scale parameters ( $N_{E1}$ ,  $N_{DL}$ ,  $Pe$ ,  $A$  and  $\lambda^*$ ) (Eqs. (1)–(2a)). The coefficients,  $a_i$ ,  $b_i$  and  $c_i$  in Eqs. (15)–(17) are here onwards called as the multipliers, and for a given soil, their values need to be found by comparing the values of the Darcy-scale deposition parameters predicted by the correlation equations (Eqs. (15)–(17)) against the estimated values of nanoparticle deposition rate coefficients from column or field experiments obtained by fitting the corresponding BTCs with 1-D advection-dispersion-deposition model.

**Table 3**

Values of coefficients in the Darcy-scale correlation equations for the deposition rate coefficients of Group I nanoparticles.

Favorability	Unfavorable ( $N_{E1} \geq 10$ )					
Coefficients of dimensionless expression <sup>a</sup>	$a_2$	−0.095	$b_2$	−0.097	$c_2$	−0.021
	$a_3$	0.326	$b_3$	0.337	$c_3$	0.08
	$a_4$	−0.184	$b_4$	−0.161	$c_4$	−0.071
	$a_5$	0.28	$b_5$	0.279	$c_5$	0.041
	$a_6$	0.163	$b_6$	0.160	$c_6$	0.067
	$a_7$	0.685	$b_7$	1.259	$c_7$	0.068
	%RMSE	4.76		1.73		12.76
$R^2$	0.96		0.96		0.84	
Coefficients of dimensional expression <sup>b</sup>	$d_2$	0.258	$e_2$	0.266	$f_2$	0.061
	$d_3$	0.115	$e_3$	0.09	$f_3$	0.053
	$d_4$	0.184	$e_4$	0.161	$f_4$	0.071
	$d_5$	0.095	$e_5$	0.097	$f_5$	0.021
	$d_6$	0.163	$e_6$	0.168	$f_6$	0.04
	$d_7$	0.184	$e_7$	0.839	$f_7$	0.071
	$d_8$	0.463	$e_8$	1.44	$f_8$	0.112
	$d_9$	0.165	$e_9$	0.198	$f_9$	0.039
	$d_{10}$	0.685	$e_{10}$	1.259	$f_{10}$	0.068

<sup>a</sup> Coefficients in Eqs. (15)–(17).

<sup>b</sup> Coefficients in Eqs. (18)–(20).

Eqs. (15)–(17) can be written in dimensional form, which results in correlation equations for  $K_{D(D)}$ ,  $k_{att(D)}$ , and  $f$  in terms of ten dimensional measurable parameters at Darcy scale ( $\varepsilon$ ,  $T$ ,  $\mu$ ,  $\psi_1$ ,  $\psi_2$ ,  $l$ ,  $\bar{v}$ ,  $\bar{R}$ ,  $a$  and  $\theta$ ) as given in Eqs. (18)–(20).

$$K_{D(D)} = d_1 \varepsilon^{-d_2} T^{d_3} \mu^{-d_4} (\psi_1^2 + \psi_2^2)^{-d_5} l^{d_6} \bar{v}^{-d_7} \bar{R}^{-d_8} a^{d_9} \theta^{d_{10}} \quad (18)$$

$$k_{att(D)} = e_1 \varepsilon^{-e_2} T^{e_3} \mu^{-e_4} (\psi_1^2 + \psi_2^2)^{-e_5} l^{e_6} \bar{v}^{e_7} \bar{R}^{-e_8} a^{e_9} \theta^{e_{10}} \quad (19)$$

$$f = \ln \left( f_1 \varepsilon^{-f_2} T^{f_3} \mu^{-f_4} (\psi_1^2 + \psi_2^2)^{-f_5} l^{f_6} \bar{v}^{-f_7} \bar{R}^{-f_8} a^{-f_9} \theta^{f_{10}} \right) \quad (20)$$

The values of constants,  $d_i$ ,  $e_i$  and  $f_i$  ( $i = 2, \dots, 10$ ), in Eqs. (18)–(20) are given in Tables 3–5. Values of coefficients  $d_i$ ,  $e_i$  and  $f_i$  depend on  $N_A$ ,  $k_B$ ,  $e$ ,  $\varepsilon_0$  and  $\lambda$ , as given below:

$$d_1 = a_1 \pi^{a_2+a_4} 2000^{a_3/2} 6^{a_4} \left[ N_A^{0.5a_3} k_B^{-(a_2+0.5a_3+a_4)} e^{a_2\varepsilon_0^{0.2-0.5a_3}\lambda^{a_6}} \right] \quad (21)$$

$$e_1 = b_1 \pi^{b_2+b_4} 2000^{b_3/2} 6^{b_4} \left[ N_A^{0.5b_3} k_B^{-(b_2+0.5b_3+b_4)} e^{b_2\varepsilon_0^{b_2-0.5b_3}\lambda^{b_6}} \right] \quad (22)$$

**Table 4**

Values of coefficients in the Darcy-scale correlation equations for the deposition rate coefficients of Group II nanoparticles.

Favorability	Unfavorable ( $N_{E1} \geq 20$ )					
Coefficients of dimensionless expression <sup>a</sup>	$a_2$	−0.099	$b_2$	−0.103	$c_2$	−0.03
	$a_3$	0.34	$b_3$	0.355	$c_3$	0.109
	$a_4$	−0.211	$b_4$	−0.187	$c_4$	−0.095
	$a_5$	0.408	$b_5$	0.444	$c_5$	0.077
	$a_6$	0.310	$b_6$	0.366	$c_6$	−0.005
	$a_7$	0.022	$b_7$	0.512	$c_7$	−0.107
	%RMSE	4.35		1.93		11.88
$R^2$	0.95		0.94		0.92	
Coefficients of dimensional expression <sup>b</sup>	$d_2$	0.269	$e_2$	0.281	$f_2$	0.084
	$d_3$	0.140	$e_3$	0.113	$f_3$	0.07
	$d_4$	0.211	$e_4$	0.187	$f_4$	0.095
	$d_5$	0.099	$e_5$	0.103	$f_5$	0.03
	$d_6$	0.17	$e_6$	0.178	$f_6$	0.055
	$d_7$	0.211	$e_7$	0.813	$f_7$	0.095
	$d_8$	0.619	$e_8$	1.632	$f_8$	0.172
	$d_9$	0.128	$e_9$	0.143	$f_9$	−0.067
	$d_{10}$	0.022	$e_{10}$	0.512	$f_{10}$	−0.107

<sup>a</sup> Coefficients in Eqs. (15)–(17).

<sup>b</sup> Coefficients in Eqs. (18)–(20).

**Table 5**  
Values of coefficients in the Darcy-scale correlation equations for the deposition rate coefficients of Group III Nanoparticles.

Favorability	Unfavorable ( $N_{E1} \geq 40$ )										
Coefficients of dimensionless expression <sup>a</sup>	$a_2$	-0.076	$b_2$	-0.076	$c_2$	-0.026					
	$a_3$	0.346	$b_3$	0.369	$c_3$	0.126					
	$a_4$	-0.194	$b_4$	-0.185	$c_4$	-0.101					
	$a_5$	0.539	$b_5$	0.601	$c_5$	0.092					
	$a_6$	0.794	$b_6$	0.900	$c_6$	0.166					
	$a_7$	0.457	$b_7$	0.957	$c_7$	0.113					
	%RMSE	3.41		1.84		15.44					
$R^2$	0.96		0.94		0.89						
Coefficients of dimensional expression <sup>b</sup>	$d_2$	0.249	$e_2$	0.26	$f_2$	0.089					
	$d_3$	0.097	$e_3$	0.076	$f_3$	0.064					
	$d_4$	0.194	$e_4$	0.185	$f_4$	0.101					
	$d_5$	0.076	$e_5$	0.076	$f_5$	0.026					
	$d_6$	0.173	$e_6$	0.185	$f_6$	0.063					
	$d_7$	0.194	$e_7$	0.815	$f_7$	0.101					
	$d_8$	0.734	$e_8$	1.785	$f_8$	0.193					
	$d_9$	-0.179	$e_9$	-0.19	$f_9$	0.075					
	$d_{10}$	0.457	$e_{10}$	0.957	$f_{10}$	0.113					

<sup>a</sup> Coefficients in Eqs. (15)–(17).

<sup>b</sup> Coefficients in Eqs. (18)–(20).

$$f_1 = c_1 \pi^{c_2+c_4} 2000^{c_3/2} 6^{c_4} \left[ N_A^{0.5c_3} k_B^{-(c_2+0.5c_3+c_4)} e^{c_3} \varepsilon_0^{c_2-0.5c_3} \lambda^{c_6} \right] \quad (23)$$

The correlation equation for  $\alpha_{(D)}$  (obtained from Eqs. (18)–(19) as  $\alpha_{(D)} = k_{att(D)}/K_{D(D)}$ ) is found to be insensitive to all parameters, except for  $\bar{v}$ ,  $\bar{R}$  and  $\theta$ .

### 6. Comparison with observed trends from literature

The trends predicted by the correlation equations (Eqs. (18)–(20)) for the Darcy-scale deposition coefficients ( $K_{D(D)}$ ,  $k_{att(D)}$ , and  $f$ ) vs the ten Darcy-scale parameters will be discussed, followed by comparison of the predicted trends with the observed trends from column-scale or batch-scale experimental data available in the literature.

#### 6.1. Effect of dielectric constant

As the solution dielectric constant increases, the electrostatic repulsive force between the particle and the collector increases. Hence, nanoparticle deposition decreases, resulting in decreasing values of  $K_{D(D)}$  and  $k_{att(D)}$  (Eqs. (18)–(19)). Also, the fraction of sites where equilibrium deposition occurs,  $f$ , decreases with increasing dielectric constant (Eq. (20)), which indicates that kinetic processes become more important under unfavorable conditions.

#### 6.2. Effect of temperature

When temperature increases, the particle diffusion coefficient increases. This increases the rate of transfer of particles to the grain surface, and hence increased deposition leading to a positive correlation between  $K_{D(D)}$  (and  $k_{att(D)}$ ) vs  $T$  (Eqs. (18)–(19)), which is also consistent with the experimental observations (Chrysikopoulos and Aravantinou, 2014; Syngouna and Chrysikopoulos, 2010), as given in Table 6.

#### 6.3. Effect of solution viscosity

Eqs. (18)–(19) show that  $K_{D(D)}$  and  $k_{att(D)}$  decrease with increasing solution viscosity. Increase in solution viscosity lowers the particle diffusion coefficient, and reduces the rate of transfer of particles to the grain surface. In addition, the drag force acting on the particle near to the grain surface increases. Hence, nanoparticle deposition decreases with increasing viscosity.

#### 6.4. Effect of ionic strength

The Darcy-scale correlation equations predict that  $K_{D(D)}$ ,  $k_{att(D)}$  and  $f$  increase with increasing solution ionic strength and decrease with increasing values of surface potentials on nanoparticle and grain surface. This trend is consistent with the column-scale experimental results found in the literature (Cai et al., 2014; Compere et al., 2001; Elimelech and O’Melia, 1990; Johnson et al., 2007b; Kang et al., 2015; Knappett et al., 2008; Li et al., 2005; Litton and Olson, 1996; Sadeghi et al., 2011; Sasidharan et al., 2014; Shen et al., 2007; Tosco et al., 2012; Tufenkji and Elimelech, 2005; Wang et al., 2012). This is due to the reduction in the electric double layer thickness around the particle and the grain surface, and the reduction in the negative surface potentials of the particle and grain surface with increasing ionic strength, thereby reducing the repulsive force between them. Table 6 shows the consistency between the trends predicted by the correlation equations and the observed trends from the literature.

#### 6.5. Effect of mean pore water velocity

Eqs. (18)–(20) predict that an increase in the mean pore water velocity causes a decrease of  $K_{D(D)}$ , increase of  $k_{att(D)}$ , and decrease of  $f$ . The expression obtained in this study for  $k_{att(D)}$  vs  $\bar{v}$  is consistent with the column experimental results of Compere et al. (2001), Kang et al. (2015), Li et al. (2008), Sasidharan et al. (2014), Seetha et al. (2015b) and Vasiliadou and Chrysikopoulos (2011), as shown in Table 6. However, there are also results from some column experiments that show that estimated values of Darcy-scale attachment rate coefficient for nanoparticles and colloids decrease with increasing pore water velocity (Keller et al., 2004; Li et al., 2005; Tong and Johnson, 2006; Tosco et al., 2012).

#### 6.6. Effect of mean pore throat radius

The diffusion length from the bulk solution toward the grain surface increases with  $\bar{R}$ . In addition, porosity and the specific surface area of the porous medium decrease with increasing  $\bar{R}$ . Hence, nanoparticle deposition decreases, resulting in a negative correlation between both  $K_{D(D)}$  and  $k_{att(D)}$  vs  $\bar{R}$ , and a positive correlation between both  $K_{D(D)}$  and  $k_{att(D)}$  vs porosity (Eqs. (18)–(19)). The fraction of sites where equilibrium deposition occur decreases with increasing pore throat radius and decreasing porosity (Eq. (20)), due to the dominance of advective transport compared to the deposition. This trend agrees with the available column experimental results as shown in Table 6 (Knappett et al., 2008; Li et al., 2008; Shen et al., 2008; Chrysikopoulos and Aravantinou, 2014).

#### 6.7. Effect of nanoparticle radius

Eqs. (18)–(19) predict a positive correlation between both  $K_{D(D)}$  and  $k_{att(D)}$  vs the nanoparticle radius for Group I and II nanoparticles and a negative correlation for Group III nanoparticles (Tables 3–5). This is due to the dominance of advective transport for larger particles at a given mean pore water velocity. This result is in contrast to column experimental observations available in the literature for nanoparticle transport in porous media. For example, Sasidharan et al. (2014), and Zhuang et al. (2005) observed decreased retention with increasing particle size for Group I and II nanoparticles. This discrepancy may be because the range of values of  $Pe_D$  used in deriving our correlation equations is 0.05–50 (pore water velocity =  $10^{-7}$ – $6 \times 10^{-6}$  m/s), while the column experiments (Sasidharan et al., 2014; Zhuang et al., 2005) were performed at  $Pe_D$  values (~100–3000) which were orders of magnitude greater than the values used in this study. The effect of nanoscale heterogeneity of the grain surface is not considered in this study, which may contribute to the increased retention of smaller particles (May and Li, 2013; Sasidharan et al., 2014). The results from this

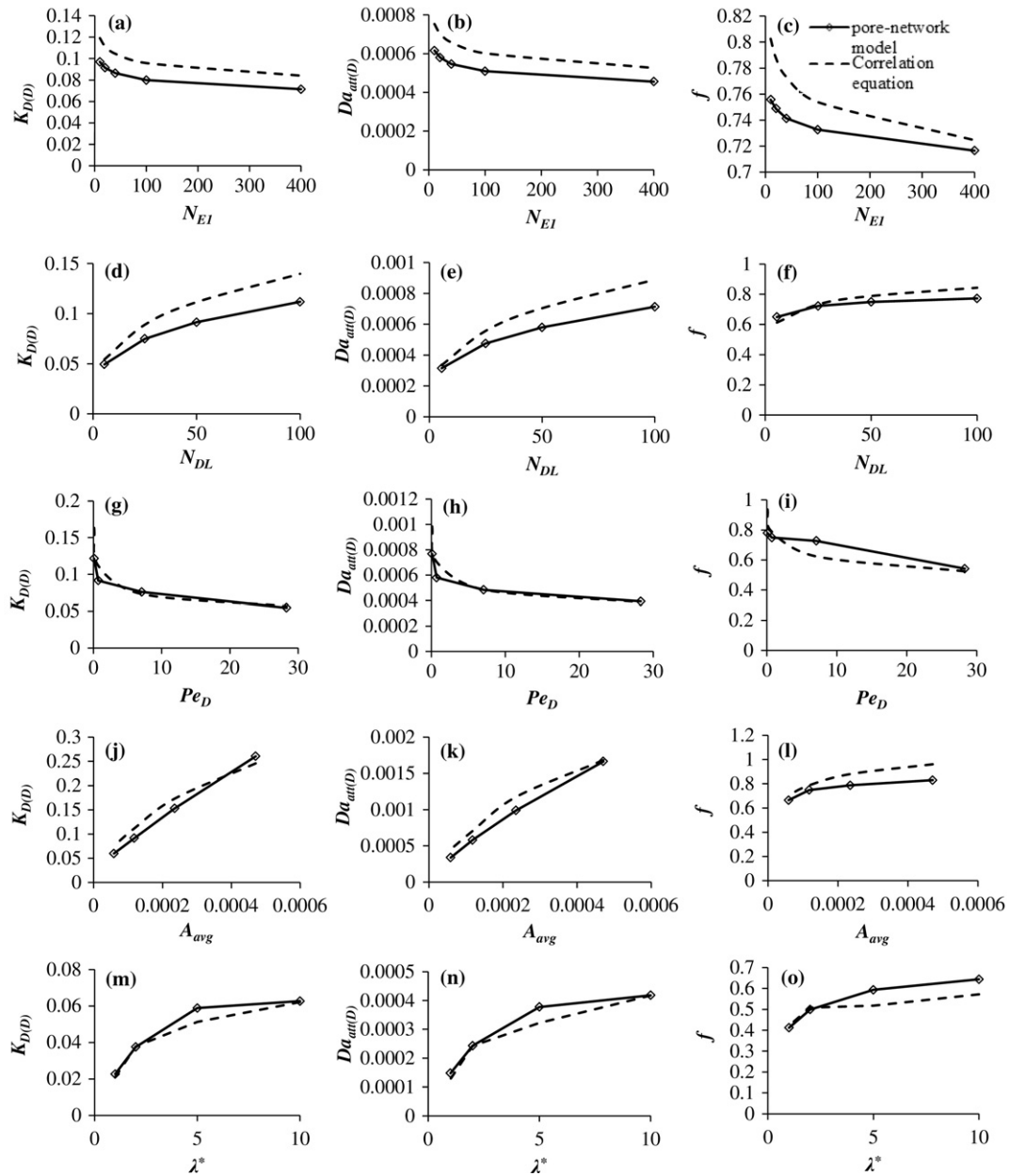


**Fig. 2.** Effect of various Darcy-scale parameters on the Darcy-scale deposition coefficients (solid line: estimated values obtained by fitting the BTCs from pore-network model, dotted line: predicted values from correlation equations). The parameters used in the simulations are, a to l:  $N_{EI} = 20$ ,  $N_{DL} = 50$ ,  $Pe_D = 0.71$ ,  $A_{avg} = 0.0001$ ,  $\lambda^* = 10$ , and  $\theta = 0.392$ , and m, n & o:  $N_{EI} = 40$ ,  $N_{DL} = 50$ ,  $Pe_D = 11.8$ , and  $A_{avg} = 0.0001$ .

study are consistent with the trends obtained from the column experimental results of Shani et al. (2008) and Tong and Johnson (2006) who studied the transport of Group I or II and Group III nanoparticles in porous media, though the value of  $Pe_D$  (~300–5000) is larger than the values used in this study (Table 6).

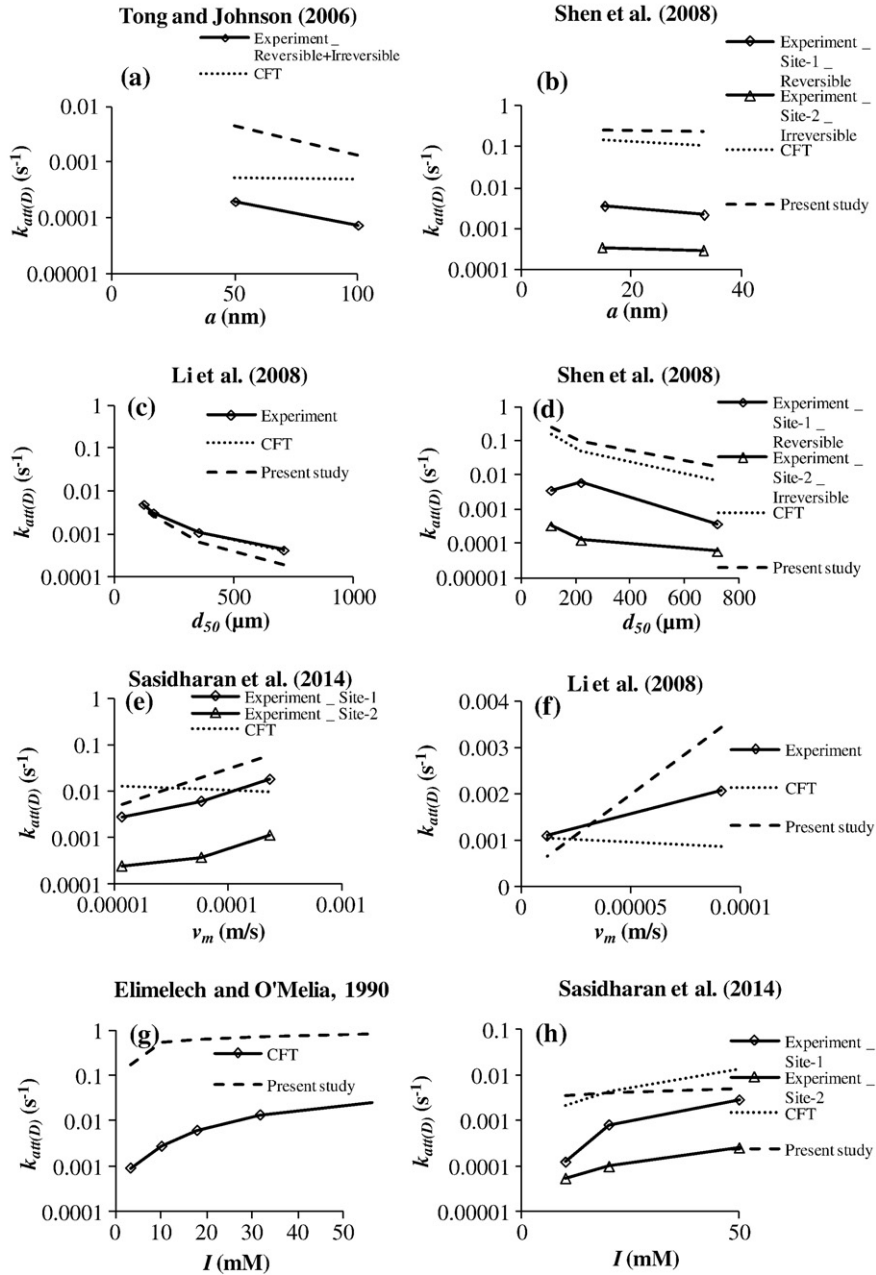
### 6.8. Comparison with experimental data

Fig. 3 compares the predicted values of attachment rate coefficient obtained from the correlation equation Eq. (19) by taking the value of multiplier,  $b_1$ , in Eq. (22) as unity, and the corresponding estimated values obtained by fitting the observed BTCs with a 1-D model for the column experimental results of Elimelech and O'Melia (1990), Li et al. (2008), Sasidharan et al. (2014), Shen et al. (2008), and Tong and Johnson (2006). Fig. 3 also shows the corresponding value of attachment rate coefficient predicted by CFT. As not every single parameter

needed to predict the Darcy-scale deposition rate coefficients using the correlation equations developed in this study is reported in the above literature, for some cases we selected the corresponding typical values (e.g.,  $\bar{R}$  is taken as equal to  $0.25d_{50}$ , where  $d_{50}$  is the median grain size). The various 1-D models that were found to fit the experimental data of the above literature are given in Table 6 (Elimelech and O'Melia, 1990, Li et al., 2008, Sasidharan et al., 2014, Shen et al., 2008, Tong and Johnson, 2006). Fig. 3 shows that the trends predicted by the Darcy-scale correlation equation (Eq. (19)) for attachment rate coefficient are consistent with the observed trends from the column experimental results, and the predicted and the observed trends are parallel to each other in most cases. This justifies the use of a multiplier in the correlation equations, and its value for a given porous medium can be found by dividing the fitted value of the attachment rate coefficient obtained from the experimental data with the predicted value from the correlation equation.

**Table 6**  
Observed trends from literature for comparison with Darcy-scale correlation equations.

Reference	Parameter studied	Type of experiment	Particle (size nm)	Porous medium	Value of parameter studied	Model	Observed trend
Syngouna and Chrysikopoulos, 2010	Temperature	Batch	MS2 (25) φX174 (26)	Kaolinite Bentonite	4 °C 25 °C	Linear isotherm	Equilibrium distribution coefficient increased when the temperature increased from 4 to 25 °C.
Chrysikopoulos and Aravantinou, 2014	Temperature	Batch	MS2 (25) φX174 (26)	Quartz sand	4 °C 20 °C	Freundlich isotherm	Freundlich constant of viruses onto quartz sand was greater at 20 °C than at 4 °C.
Compere et al., 2001	Ionic strength	Column experiment	Smectite (260)	Very fine quartz sand	$8.5 \times 10^{-5}$ – $7.62 \times 10^{-4}$ M (CaCl <sub>2</sub> )	A first-order two-site kinetic model with reversible and irreversible deposition sites	The ratio of the attachment to the detachment rate coefficient, and the attachment rate coefficients at both reversible and irreversible sites increased with increasing ionic strength.
Elimelech and O'Melia, 1990	Ionic strength	Column experiment	Polystyrene latex particles (46–753)	Glass beads	0.001–0.1 M	CFT	Deposition rate increased with increasing ionic strength under unfavorable conditions.
Tufenkji and Elimelech, 2005	Ionic strength	Column experiment	Polystyrene latex colloids (63, 320, 3000)	Soda-lime glass beads	3–300 mM KCl	CFT	Deposition increased with increasing ionic strength under unfavorable conditions.
Sadeghi et al., 2011	Ionic strength	Column experiment	PRD1 (62)	Quartz sand	1, 10 and 20 mM	Linear reversible kinetic deposition	Attachment rate coefficient increased with increasing solution ionic strength.
Wang et al., 2012	Ionic strength	Column experiment	Silica nanoparticles (8, 52)	Accusand	1, 100 mM NaCl	CFT	Attachment rate coefficient increased with increasing ionic strength.
Sasidharan et al., 2014	Ionic strength	Column experiment	Carboxyl-modified latex nanoparticles (50, 100 nm)	River sand	10–60 mM NaCl, 0.5–3 mM CaCl <sub>2</sub>	Two-site kinetic model accounting for irreversible deposition and blocking on each site	Attachment rate coefficients at both the sites increased with increasing solution ionic strength.
Kang et al., 2015	Ionic strength	Column experiment	Carboxyl-functionalized carbon black nanoparticles (77.2)	Quartz sand	0.1, 1 mM NaCl, 0.01–0.1 mM CaCl <sub>2</sub>	First-order irreversible model	Attachment rate coefficient increased with increasing solution ionic strength.
Compere et al., 2001	Flow velocity	Column experiment	Smectite (260)	Very fine quartz sand	$1.27 \times 10^{-5}$ –0.0001 m/s	A first-order two-site kinetic model with reversible and irreversible deposition sites	The ratio of the attachment to the detachment rate coefficient decreased, and the attachment rate coefficients at reversible and irreversible sites increased with increasing pore water velocity.
Li et al., 2008	Flow velocity	Column experiment	Nanoscale fullerene aggregate (120)	Ottawa sand	$1.16 \times 10^{-5}$ – $9.3 \times 10^{-5}$ m/s	One-site irreversible kinetic model with blocking	Attachment rate coefficient increased and the maximum retention capacity decreased as the pore water velocity increased.
Vasiliadou and Chrysikopoulos, 2011	Flow velocity	Column experiment	Pseudomonas putida Kaolinite	Glass beads	$1.6 \times 10^{-4}$ $2.43 \times 10^{-4}$ $3.25 \times 10^{-4}$ m/s	First-order reversible kinetic model	Attachment rate coefficient increased, and the ratio of attachment to detachment rate coefficients decreased with increasing pore water velocity.
Sasidharan et al., 2014	Flow velocity	Column experiment	Carboxyl-modified latex nanoparticles (50, 100 nm)	Natural graded river sand	$1.16 \times 10^{-5}$ – $2.3 \times 10^{-4}$ m/s	Two-site kinetic model that accounted for irreversible deposition and blocking on each site	Attachment rate coefficients at both the sites increased and the fraction of the solid surface area available for deposition decreased with increasing flow velocity.
Kang et al., 2015	Flow velocity	Column experiment	Carboxyl-functionalized carbon black nanoparticles (77.2)	Quartz sand	$2.2 \times 10^{-5}$ – $4.5 \times 10^{-5}$ m/s	First-order irreversible model	Attachment rate coefficient increased with increasing pore water velocity.
Syngouna and Chrysikopoulos, 2013 and Seetha et al. (2015b)	Flow velocity	Column experiment	MS2 (25) φX174 (26)	Glass bead	$6.33 \times 10^{-5}$ – $2 \times 10^{-4}$ m/s	Linear reversible kinetic model	Attachment rate coefficient increased, and the ratio of attachment to detachment rate coefficients decreased as the pore water velocity increased.
Knappett et al., 2008	Grain size	Column experiment	MS2 (25)	Angular silica sand	0.34–0.7 mm	Linear irreversible kinetic model	The estimated first-order kinetic attachment rate coefficient in fine sand ( $d_{50} = 0.34$ mm) is greater than that in the medium sand ( $d_{50} = 0.7$ mm).
Li et al., 2008	Grain size	Column experiment	Nanoscale fullerene aggregate (120)	Ottawa sand	0.125–0.710 mm	One-site irreversible kinetic model with blocking	Attachment rate coefficient and the maximum retention capacity of the porous medium decreased with increasing mean sand size.
Shen et al., 2008	Grain size	Column experiment	Carboxyl-modified latex microspheres (33, 66)	Glass beads	0.11 0.22 0.72 mm	Two-site kinetic model with reversible and irreversible sites	Attachment rate coefficients at both the sites decreased with increasing grain size.
Chrysikopoulos and Aravantinou, 2014	Grain size	Batch	MS2 (25) φX174 (26)	Quartz sand	0.181 mm 0.513 mm 1.44 mm	Freundlich isotherm	Freundlich constant for viruses decreased with increasing quartz sand size.
Tong and Johnson, 2006	Particle size	Column experiment	Carboxylate-modified latex microspheres (100, 200)	Glass beads	100 200 nm	Two-site linear kinetic model with reversible and irreversible sites	Estimated value of attachment rate coefficient decreased with increasing particle size at a velocity of 4 m/d.
Shani et al., 2008	Particle size	Column experiment	Fluorescent microspheres (20, 200)	Natural dune sand	20 200 nm	–	Effluent peak breakthrough concentration increased, and hence the deposition decreased with increasing particle size.



**Fig. 3.** Values of attachment rate coefficient vs various measurable Darcy-scale parameters from column experiments (Dashed lines: Predicted values from correlation Eq. (19), dotted lines: predicted values from CFT, and solid lines: estimated values obtained by fitting the observed BTCs with a 1-D model). The values of parameters are (a)  $v_m = 4$  m/d, (b)  $d_{50} = 110$   $\mu\text{m}$ , (c)  $v_m = 8$  m/d, (d)  $a = 15$  nm, (e)  $a = 25$  nm,  $I_S = 50$  mM, (f)  $d_{50} = 355$   $\mu\text{m}$ , (g)  $a = 121$  nm, and (h)  $a = 25$  nm,  $v_m = 1$  m/d. The values of other parameters are taken as given in the corresponding literature. The 1-D models that correspond to the various column experimental data used here are given in Table 6.

## 7. Darcy-scale correlation equation versus colloid filtration theory

In this section, we compare the Darcy-scale correlation equation for the attachment rate coefficient under unfavorable conditions developed in this paper (Eq. (19)) with the Colloid Filtration Theory, which describes colloid attachment to the grain surface by a first-order irreversible kinetic model as (Tufenkji and Elimelech, 2004; Yao et al., 1971):

$$k_{att(CFT)} = \frac{3(1-\theta)}{2} \frac{\bar{v}}{d_c} \bar{v} \alpha \eta_0 \quad (24)$$

Here,  $k_{att(CFT)}$  is the Darcy-scale attachment rate coefficient prescribed by CFT, and  $d_c$  is the average grain diameter. As diffusion is the dominant transport mechanism for nanoparticle deposition onto the grain surface,

the total single collector efficiency ( $\eta_0$ ) is approximately equal to the single collector efficiency due to diffusion ( $\eta_D$ ) (i.e.,  $\eta_0 \approx \eta_D$ ). Tufenkji and Elimelech (2004) and Bai and Tien (1999), based on theoretical and empirical considerations, developed the following correlation equations for  $\eta_D$  and  $\alpha$  (Seetha et al., 2015a):

$$\eta_D \propto T^{0.663} \mu^{-0.715} \bar{v}^{-0.715} R^{-0.634} a^{-0.796} \quad (25)$$

$$\alpha \propto \varepsilon^{-0.9881} T^{-0.676} (\psi_1^2 + \psi_2^2)^{-0.3121} I^{0.676} \mu^{-0.391} \bar{v}^{-0.391} a^{0.2579} \quad (26)$$

Substituting for  $\eta_0$  and  $\alpha$  in Eq. (24) from Eqs. (25)–(26), respectively, results in the following expression for the Darcy-scale attachment rate

coefficient prescribed by CFT (Seetha et al., 2015a).

$$k_{att(D)} \propto \varepsilon^{-0.9881} T^{-0.013} \mu^{-1.106} (\psi_1^2 + \psi_2^2)^{-0.3121} I^{0.676} \bar{v}^{-0.106} \bar{R}^{-1.634} a^{-0.5381} \quad (27)$$

Comparison of Eqs. (19) and (27) indicates that they both show the same trends for all parameters, except for  $\bar{v}$ ,  $a$  and  $T$ . The inconsistency for  $\bar{v}$  and  $a$  may be due to the different range of values of  $\bar{v}$  and  $a$  used in the simulations performed in this study ( $\bar{v} = 10^{-7}$ – $6 \times 10^{-6}$  m/s;  $a = 10$ – $100$  nm) and in deriving the correlation equations for  $\eta_0$  by Tufenkji and Elimelech (2004) ( $\bar{v} = 1.9 \times 10^{-5}$ – $0.0056$  m/s;  $a = 10$  nm– $10 \mu\text{m}$ ) and  $\alpha$  by Bai and Tien (1999) (Darcy velocity =  $0.001$ – $0.004$  m/s;  $a = 30$  nm– $5.7 \mu\text{m}$ ). This is also supported by Fig. 3 which compares the values of Darcy-scale attachment rate coefficient predicted by CFT (Eq. (24)) for various column experimental data from literature (Elimelech and O'Melia, 1990; Li et al., 2008; Sasidharan et al., 2014; Shen et al., 2008; Tong and Johnson, 2006) with the corresponding values obtained from the correlation equation Eq. (19).

Empirical expressions for the attachment efficiency,  $\alpha$ , for Group I, II and III nanoparticles can be derived by comparing Eqs. (19) and (24), with  $\eta_0$  being substituted with Eq. (25). We obtain:

$$\alpha \propto \varepsilon^{-0.266} T^{-0.626} (\psi_1^2 + \psi_2^2)^{-0.097} I^{0.168} \mu^{0.554} \bar{v}^{0.554} \bar{R}^{0.194} a^{0.994} \quad (28)$$

$$\alpha \propto \varepsilon^{-0.281} T^{-0.603} (\psi_1^2 + \psi_2^2)^{-0.103} I^{0.178} \mu^{0.528} \bar{v}^{0.528} \bar{R}^{0.002} a^{0.939} \quad (29)$$

$$\alpha \propto \varepsilon^{-0.261} T^{-0.6385} (\psi_1^2 + \psi_2^2)^{-0.076} I^{0.185} \mu^{0.53} \bar{v}^{0.53} \bar{R}^{-0.151} a^{0.606} \quad (30)$$

The trend predicted by Eqs. (28)–(30) for the various parameters are consistent with the empirical correlation for  $\alpha$  derived by Bai and Tien (1999) (Eq. (26)), except for  $\bar{v}$  and  $\mu$ . A reason for this discrepancy for  $\bar{v}$  may be due to the large values of velocity (Darcy velocity =  $0.001$ – $0.004$  m/s) used in deriving the empirical correlation equation (Eq. (26)) as compared to the values used in this study. In this regard, conflicting results are found in the literature. Many researchers have observed, from column experiments, that the experimental attachment efficiency decreases with increasing pore water velocity (Anders and Chrysikopoulos, 2005; Johnson et al., 2007b; Keller et al., 2004; Shen et al., 2010; Tong and Johnson, 2006). But, column experimental results of Sasidharan et al. (2014), Syngouna and Chrysikopoulos (2013), and Vasiliadou and Chrysikopoulos (2011) show that the attachment efficiency (calculated using Eq. (24), knowing the fitted value of attachment rate coefficient) increases with increasing pore water velocity. The positive correlation predicted by Eqs. (28)–(30) for  $\bar{v}$  are also consistent with the study of Kim and Lee (2014), who performed column experiments to study the transport of titanium dioxide nanoparticles through sand at low range of values of pore water velocities ( $\bar{v} = 2.4 \times 10^{-6}$ – $4.9 \times 10^{-4}$  m/s) which are more relevant to typical field conditions. The experimental attachment efficiency was found to increase with increasing pore water velocity (Kim and Lee, 2014). This is believed to be due to the increased mass transfer of nanoparticles to the sand surface with increasing flow velocity, resulting in a higher chance of particle collisions, and therefore an increase in  $\alpha$ . Kim and Lee (2014) observed that the empirical correlation equation available in the literature (Bai and Tien, 1999), which predict decreasing values of  $\alpha$  with increasing flow velocity, is applicable only for pore water velocities  $> 4 \times 10^{-4}$  m/s. Pelley and Tufenkji (2008) found from column experiments that, under unfavorable conditions, the experimental attachment efficiencies of latex nanoparticles (with diameters 50, 110 and 1500 nm) onto quartz sand increased with increasing particle size. Litton and Olson (1996) studied the influence of particle size on the deposition kinetics of carboxyl latex microspheres (with diameters 245,

481 and 755 nm) in granular quartz beds, and found the experimental attachment efficiency to follow a positive correlation with particle size. Both of above studies attributed the increased particle deposition with particle size to the contribution of secondary minimum deposition for larger particles. This supports the trend predicted by Eqs. (28)–(30).

## 8. Conclusions

In this study, we upscaled nanoparticle transport from pore to the Darcy scale by incorporating the correlations equations for the pore-averaged deposition rate coefficients of nanoparticles under unfavorable conditions (developed by Seetha et al. (2015a)) into a multi-directional pore-network model, PoreFlow (Raouf et al., 2013). Breakthrough curves of nanoparticles obtained from the pore-network model are described using a 1-D advection-dispersion equation, with deposition being described by a two-site linear reversible model with terms accounting for both equilibrium and kinetic sorption. Correlation equations for the Darcy-scale deposition coefficients of nanoparticles under unfavorable conditions are derived as a function of ten measurable Darcy-scale parameters, including: porosity, mean pore throat radius, mean pore water velocity, nanoparticle radius, ionic strength, dielectric constant, viscosity, temperature, and surface potentials of the particle and grain surfaces. The correlation equations developed in this study are valid for the cases where nanoparticle deposition onto the grain surface is described using a two-site model accounting for both equilibrium and kinetic sorption. The Darcy-scale correlation equations for the distribution coefficient and the attachment rate coefficient show a positive correlation with porosity, ionic strength, and temperature, whereas a negative correlation is found with mean pore throat radius, dielectric constant, viscosity, and surface potentials of the particle and grain surfaces. The Darcy-scale distribution coefficient decreases with increasing mean pore water velocity, whereas the attachment rate coefficient follows the opposite trend. Nanoparticle deposition at Darcy scale is found to have a positive correlation with nanoparticle radius for small particles, and a negative correlation for large particles due to the greater effect of hydrodynamic forces on larger particles. Kinetic sorption is found to become important as the favorability of the surface for deposition decreases. The correlation equations are found to be consistent with the observed trends from column experiments available in the literature, and are in agreement with colloid filtration theory for all parameters, except for the mean pore water velocity and nanoparticle radius. This discrepancy may be due to the different range of values of pore water velocity and particle radius considered in this study and in the CFT. We also derived expressions for attachment efficiency in terms of the ten measurable Darcy-scale parameters. The Darcy-scale empirical formulas developed in this study contain free multipliers whose values need to be determined from calibration.

## 9. Notation

$a$	nanoparticle radius [L]
$A$	interception parameter [-]
$A_{avg}$	average interception parameter [-]
$A_c$	cross-sectional area of the network perpendicular to the overall flow direction [L <sup>2</sup> ]
$c_i$	average nanoparticle concentration in the pore body $i$ [no. L <sup>-3</sup> ]
$c_{ij}$	average nanoparticle concentration in the pore throat $ij$ [no. L <sup>-3</sup> ]
$c_0$	inlet nanoparticle concentration to the network [no. L <sup>-3</sup> ]
$\bar{c}$	nanoparticle breakthrough concentration from the pore network [no. L <sup>-3</sup> ]
$Da_{att}, Da_{det}$	Damköhler numbers corresponding to the rate coefficient for nanoparticle attachment to and detachment from the pore wall in a cylindrical pore [-]
$d_c$	average grain diameter [L]

$D_L$	dispersion coefficient at Darcy scale [ $L^2 T^{-1}$ ]
$D_\infty$	particle bulk diffusion coefficient [ $L^2 T^{-1}$ ]
$e$	elementary charge [IT]
$f$	fraction of sites assumed to be in equilibrium with the liquid phase at Darcy scale [-]
$I$	solution ionic strength [Molar]
$k_{att}, k_{det}$	average rate coefficients for nanoparticle attachment and detachment in a cylindrical pore [ $T^{-1}$ ]
$k_{att}(CFT)$	Darcy-scale attachment rate coefficient prescribed by CFT [ $T^{-1}$ ]
$k_{att}(D)$	rate coefficient for nanoparticle attachment at Darcy scale [ $T^{-1}$ ]
$k_{att,ij}$	attachment rate coefficient in the pore throat $ij$ [ $T^{-1}$ ]
$k_B$	Boltzmann constant [ $M L^2 T^{-2} \theta^{-1}$ ]
$K_{d,ij}$	equilibrium distribution coefficient in the pore throat $ij$ [-]
$K_D$	equilibrium distribution coefficient in a cylindrical pore in the model of Seetha et al. (2015a) [L]
$K'_D$	dimensionless equilibrium distribution coefficient in a cylindrical pore in the model of Seetha et al. (2015a) [-]
$K_D(D)$	Darcy-scale equilibrium distribution coefficient [-]
$l$	length of the pore throat [L]
$L$	network length [L]
$N_A$	Avogadro number [-]
$N_{E1}$	dimensionless parameter representing the magnitudes of surface potentials [-]
$N_{DL}$	dimensionless parameter representing the ratio of nanoparticle radius to double layer thickness [-]
$N_{in}$	number of pore throats flowing into the pore body $i$ [-]
$N_t$	number of pore bodies at the outlet boundary of the network [-]
$P_i$ and $P_j$	pressures at pore bodies $i$ and $j$ , respectively [ $ML^{-1} T^{-2}$ ]
$Pe$	Péclet number of a cylindrical pore [-]
$Pe_D$	Average network Péclet number [-]
$q_{ij}$	discharge through a given pore throat $ij$ [ $L^3 T^{-1}$ ]
$Q$	total discharge through the network [ $L^3 T^{-1}$ ]
$Q_i$	total water flux leaving the pore body $i$ [ $L^3 T^{-1}$ ]
$R$	radius of cylindrical pore [L]
$\bar{R}$	mean pore throat radius [L]
$R_{ij}$	radius of the pore throat connecting pore bodies $i$ and $j$ [L]
$\bar{R}_{pb}$	mean pore body radius [L]
$s_{ij}$	average attached concentration in the pore throat $ij$ [no. $L^{-3}$ ]
$\bar{s}$	average nanoparticle attached concentration at Darcy scale [no. $L^{-3}$ ]
$\bar{s}_e$	average attached concentration at the equilibrium site at Darcy scale [no. $L^{-3}$ ]
$\bar{s}_k$	average attached concentration at the kinetic site at Darcy scale [no. $L^{-3}$ ]
$T$	absolute temperature [ $\theta$ ]
$v_m$	mean flow velocity in cylindrical pore [ $LT^{-1}$ ]
$\bar{v}$	average water velocity through the network [ $LT^{-1}$ ]
$V_i$	volume of the pore body $i$ [ $L^3$ ]
$V_{ij}$	volume of the pore throat $ij$ [ $L^3$ ]
$z_i$	coordination number of the pore body $i$ [-]
$\alpha$	attachment efficiency [-]
$\alpha_{(D)}$	first-order kinetic rate constant equal to the detachment rate coefficient at Darcy scale [ $T^{-1}$ ]
$\alpha_{ij}$	first-order kinetic rate constant equal to the detachment rate coefficient in the pore throat $ij$ [ $T^{-1}$ ]
$\varepsilon$	dielectric constant of water [-]
$\varepsilon_0$	permittivity of vacuum [ $I^2 T^4 M^{-1} L^{-3}$ ]
$\kappa$	inverse Debye-Huckel length [ $L^{-1}$ ]
$\lambda$	characteristic wavelength of the interaction [L]
$\lambda^*$	dimensionless parameter representing the ratio of characteristic wavelength of the interaction to nanoparticle radius [-]
$\mu$	dynamic viscosity of water [ $ML^{-1} T^{-1}$ ]
$\eta_D$	single collector efficiency due to diffusion [-]

$\eta_0$	total single collector contact efficiency [-]
$\psi_1, \psi_2$	surface potentials on the nanoparticle and collector [ $ML^2 T^{-1} T^{-3}$ ]
$\theta$	porosity [-]

## Acknowledgements

The first author acknowledges the funds and facilities for six months provided by Utrecht University, The Netherlands (grant no. WA.146130.4 and Short stay fellowship 2011 for PhD candidates) to carry out a part of this work in the Department of Earth Sciences, Utrecht University. SMH received funding from the European Research Council under the European Union's Seventh Framework Programme (FP/2007-2013)/ERC Grant Agreement No. 341225. Comments and suggestions by the Editor Prof. Michael Annable and an anonymous reviewer helped to improve the manuscript significantly.

## References

- Acharya, R.C., Van der Zee, S.E.A.T.M., Leijnse, A., 2007. Approaches for modeling longitudinal dispersion in pore-networks. *Adv. Water Resour.* 30:261–272. <http://dx.doi.org/10.1016/j.advwatres.2005.11.015>.
- Anders, R., Chrysikopoulos, C.V., 2005. Virus fate and transport during artificial recharge recycled water. *Water Resour. Res.* 41:W0415. <http://dx.doi.org/10.1029/2004WR003419>.
- Armatas, G.S., 2006. Determination of the effects of the pore size distribution and pore connectivity distribution on the pore tortuosity and diffusive transport in model porous networks. *Chem. Eng. Sci.* 61:4662–4675. <http://dx.doi.org/10.1016/j.ces.2006.02.036>.
- Bai, R., Tien, C., 1999. Particle deposition under unfavorable surface interactions. *J. Colloid Interface Sci.* 218:488–499. <http://dx.doi.org/10.1006/jcis.1999.6424>.
- Bijeljic, B., Blunt, M.J., 2007. Pore-scale modeling of transverse dispersion in porous media. *Water Resour. Res.* 43, W12S11. <http://dx.doi.org/10.1029/2006WR005700>.
- Bijeljic, B., Muggeridge, A.H., Blunt, M.J., 2004. Pore-scale modeling of longitudinal dispersion. *Water Resour. Res.* 40, W11501. <http://dx.doi.org/10.1029/2004WR003567>.
- Bradford, S.A., Torkzaban, S., 2008. Colloid transport and retention in unsaturated porous media: a review of interface-, collector-, and pore-scale processes and models. *Vadose Zone J.* 7, 667–681.
- Cai, L., Tong, M., Wang, X., Kim, H., 2014. Influence of clay particles on the transport and retention of titanium dioxide nanoparticles in quartz sand. *Environ. Sci. Technol.* 48:7323–7332. <http://dx.doi.org/10.1021/es5019652>.
- Chang, Y.I., Chan, H.C., 2008. Correlation equation for predicting filter coefficient under unfavorable deposition conditions. *AIChE J.* 54 (5):1235–1253. <http://dx.doi.org/10.1002/aic.11466>.
- Chrysikopoulos, C.V., Aravantinou, A.F., 2014. Virus attachment onto quartz sand: role of grain size and temperature. *J. Environ. Chem. Eng.* 2:796–801. <http://dx.doi.org/10.1016/j.jece.2014.01.025>.
- Comper, F., Porel, G., Delay, F., 2001. Transport and retention of clay particles in saturated porous media. Influence of ionic strength and pore velocity. *J. Contam. Hydrol.* 49:1–21. [http://dx.doi.org/10.1016/S0169-7722\(00\)00184-4](http://dx.doi.org/10.1016/S0169-7722(00)00184-4).
- DeNovio, N.M., Saiers, J.E., Ryan, J.N., 2004. Colloid movement in unsaturated porous media: Recent advances and future directions. *Vadose Zone J.* 3, 338–351.
- Derjaguin, B.V., Landau, L.D., 1941. Theory of the stability of strongly charged lyophobic sols and of the adhesion of strongly charged particles in solutions of electrolytes. *Prog. Surf. Sci.* 43, 30–59.
- Elimelech, M., 1992. Predicting collision efficiencies of colloidal particles in porous media. *Water Resour. Res.* 26 (1):1–8. [http://dx.doi.org/10.1016/0043-1354\(92\)90104-C](http://dx.doi.org/10.1016/0043-1354(92)90104-C).
- Elimelech, M., O'Melia, C.R., 1990. Effect of particle size on collision efficiency in the deposition of brownian particles with electrostatic energy barriers. *Langmuir* 6 (6), 1153–1163.
- Johnson, W.P., Li, X., Assemi, S., 2007b. Deposition and re-entrainment dynamics of microbes and non-biological colloids during non-perturbed transport in porous media in the presence of an energy barrier to deposition. *Adv. Water Resour.* 30:1432–1454. <http://dx.doi.org/10.1016/j.advwatres.2006.05.020>.
- Johnson, W.P., Tong, M., Li, X., 2007a. On colloid retention in saturated porous media in the presence of energy barriers: The failure of  $\alpha$ , and opportunities to predict  $\eta$ . *Water Resour. Res.* 43, W12S13. <http://dx.doi.org/10.1029/2006WR005770>.
- Kamai, T., Nassar, M.K., Nelson, K.E., Ginn, T.R., 2015. Colloid filtration prediction by mapping the correlation-equation parameters from transport experiments in porous media. *Water Resour. Res.* 51, 8995–9012.
- Kang, J., Yi, I., Park, J., Kim, S., Kim, H., Han, Y., Kim, P., Eom, I., Jo, E., 2015. Transport of carboxyl-functionalized carbon black nanoparticles in saturated porous media: Column experiments and model analyses. *J. Contam. Hydrol.* 177–178:194–205. <http://dx.doi.org/10.1016/j.jconhyd.2015.04.009>.
- Keller, A.A., Sirivithayapakorn, S., Chrysikopoulos, C.V., 2004. Early breakthrough of colloids and bacteriophage MS2 in a water-saturated sand column. *Water Resour. Res.* 40 (8), W08304. <http://dx.doi.org/10.1029/2003WR002676>.

- Kim, C., Lee, S., 2014. Effect of seepage velocity on the attachment efficiency of TiO<sub>2</sub> nanoparticles in porous media. *J. Hazard. Mater.* 279:163–168. <http://dx.doi.org/10.1016/j.jhazmat.2014.06.072>.
- Kim, Y.S., Whittle, A.J., 2006. Filtration in a porous granular medium: 2. Application of bubble model to 1-D column experiments. *Transp. Porous Med.* 65:309–335. <http://dx.doi.org/10.1007/s11242-005-6060-0>.
- Knappett, P.S., Emelko, M.B., Zhuang, J., McKay, L.D., 2008. Transport and retention of a bacteriophage and microspheres in saturated, angular porous media: effects of ionic strength and grain size. *Water Res.* 42 (16):4368–4378. <http://dx.doi.org/10.1016/j.watres.2008.07.041>.
- Knutson, C., Valocchi, A., Werth, C., 2007. Comparison of continuum and pore-scale models of nutrient biodegradation under transverse mixing conditions. *Adv. Water Resour.* 30:1421–1431. <http://dx.doi.org/10.1016/j.advwatres.2006.05.012>.
- Lee, J., Koplik, J., 2001. Network model for deep bed filtration. *Phys. Fluids* 13 (5): 1076–1086. <http://dx.doi.org/10.1063/1.1359747>.
- Li, L., Peters, C.A., Celia, M.A., 2006. Upscaling geochemical reaction rates using pore-scale network modeling. *Adv. Water Resour.* 29:1351–1370. <http://dx.doi.org/10.1016/j.advwatres.2005.10.011>.
- Li, S., Raouf, A., Schotting, R., 2014. Solute dispersion under electric and pressure driven flows; pore scale processes. *J. Hydrol.* 517:1107–1113. <http://dx.doi.org/10.1016/j.jhydrol.2014.06.049>.
- Li, Y., Wang, Y., Pennell, K.D., Abriola, L.M., 2008. Investigation of the transport and deposition of fullerene (C<sub>60</sub>) nanoparticles in quartz sands under varying flow conditions. *Environ. Sci. Technol.* 42:7174–7180. <http://dx.doi.org/10.1021/es801305y>.
- Li, X., Zhang, P., Lin, C.L., Johnson, W.P., 2005. Role of hydrodynamic drag on microsphere deposition and re-entrainment in porous media under unfavorable conditions. *Environ. Sci. Technol.* 39:4012–4020. <http://dx.doi.org/10.1021/es048814t>.
- Litton, G.M., Olson, T.M., 1996. Particle size effects on colloid deposition kinetics: evidence of secondary minimum deposition. *Colloids Surf. A Physicochem. Eng. Asp.* 107: 273–283. [http://dx.doi.org/10.1016/0927-7757\(95\)03343-2](http://dx.doi.org/10.1016/0927-7757(95)03343-2).
- Logan, B.E., Jewett, D.G., Arnold, R.G., Bouwer, E.J., O'elia, C.R., 1995. Clarification of clean-bed filtration models. *J. Environ. Eng.* 121 (12), 869–873.
- Long, W., Hilpert, M., 2009. A correlation for the collector efficiency of brownian particles in clean-bed filtration in sphere packings by a lattice-boltzmann method. *Environ. Sci. Technol.* 43:4419–4424. <http://dx.doi.org/10.1021/es8024275>.
- Ma, H., Hradisky, M., Johnson, W.P., 2013. Extending applicability of correlation equations to predict colloidal retention in porous media at low fluid velocity. *Environ. Sci. Technol.* 47 (5):2272–2278. <http://dx.doi.org/10.1021/es304753r>.
- Ma, H., Pazmino, E., Johnson, W.P., 2011. Surface heterogeneity on hemispheres-in-cell model yields all experimentally-observed non-straining colloid retention mechanisms in porous media in the presence of energy barriers. *Langmuir* 27: 14982–14994. <http://dx.doi.org/10.1021/la203587j>.
- May, R., Li, Y., 2013. The effects of particle size on the deposition of fluorescent nanoparticles in porous media: Direct observation using laser scanning cytometry. *Colloids Surf. A Physicochem. Eng. Aspects* 418:84–91. <http://dx.doi.org/10.1016/j.colsurfa.2012.11.028>.
- Meile, C., Tuncay, K., 2006. Scale dependence of reaction rates in porous media. *Adv. Water Resour.* 29:62–71. <http://dx.doi.org/10.1016/j.advwatres.2005.05.007>.
- Messina, F., Marchisio, D.L., Sethi, R., 2015. An extended and total flux normalized correlation equation for predicting single-collector efficiency. *J. Colloid Interface Sci.* 446: 185–193. <http://dx.doi.org/10.1016/j.jcis.2015.01.024>.
- Molnar, L.L., Johnson, W.P., Gerhard, J.L., Willson, C.S., O'Carroll, D.M., 2015. Predicting colloid transport through saturated porous media: a critical review. *Water Resour. Res.* 51:6804–6845. <http://dx.doi.org/10.1002/2015WR017318>.
- Nelson, K.E., Ginn, T.R., 2011. New collector efficiency equation for colloid filtration in both natural and engineered flow conditions. *Water Resour. Res.* 47, W05543. <http://dx.doi.org/10.1029/2010WR009587>.
- Niasar, V.J., Hassanizadeh, S.M., Pyrak-Nolte, L.J., Berentsen, C., 2009. Simulating drainage and imbibition experiments in a high-porosity micromodel using an unstructured pore network model. *Water Resour. Res.* 45, W02430. <http://dx.doi.org/10.1029/2007WR006641>.
- Niasar, V.J., Prodanović, M., Wildenschild, D., Hassanizadeh, S.M., 2010. Network model investigation of interfacial area, capillary pressure and saturation relationships in granular porous media. *Water Resour. Res.* 46, W06526. <http://dx.doi.org/10.1029/2009WR008585>.
- Park, Y., Atwill, E.R., Ho, L., Packman, A.I., Harter, T., 2012. Deposition of *Cryptosporidium parvum* oocysts in porous media: A synthesis of attachment efficiencies measured under varying environmental conditions. *Environ. Sci. Technol.* 46:9491–9500. <http://dx.doi.org/10.1021/es300564w>.
- Pelley, A.J., Tufenkji, N., 2008. Effect of particle size and natural organic matter on the migration of nano and microscale latex particles in saturated porous media. *J. Colloid Interface Sci.* 321:74–83. <http://dx.doi.org/10.1016/j.jcis.2008.01.046>.
- Petosa, A.R., Jaisi, D.P., Quevedo, I.R., Elimelech, M., Tufenkji, N., 2010. Aggregation and deposition of engineered nanoparticles in aquatic environments: Role of physicochemical interactions. *Environ. Sci. Technol.* 44:6532–6549. <http://dx.doi.org/10.1021/es100598h>.
- Qin, C., Hassanizadeh, S.M., 2015. Pore-network modeling of solute transport and biofilm growth in porous media. *Transp. Porous Media* 110:345–367. <http://dx.doi.org/10.1007/s11242-015-0546-1>.
- Raeesi, B., Piri, M., 2009. The effects of wettability and trapping on relationships between interfacial area, capillary pressure and saturation in porous media: a pore-scale network modeling approach. *J. Hydrol.* 376:337–352. <http://dx.doi.org/10.1016/j.jhydrol.2009.07.060>.
- Rajagopalan, R., Tien, C., 1976. Trajectory analysis of deep-bed filtration with the sphere-in-cell porous media model. *AIChE J.* 22 (3):523–533. <http://dx.doi.org/10.1002/aic.690220316>.
- Raouf, A., 2011. *Reactive/Adsorptive Transport in (Partially-) Saturated Porous Media*. PhD Thesis. Dep. of Earth Sci., Utrecht University, Utrecht, The Netherlands.
- Raouf, A., Hassanizadeh, S.M., 2009. A new method for generating pore-network models of porous media. *Transp. Porous Media* 81:391–407. <http://dx.doi.org/10.1007/s11242-009-9412-3>.
- Raouf, A., Hassanizadeh, S.M., 2010. Upscaling transport of adsorbing solutes in porous media. *J. Porous Med.* 13 (5), 395–408.
- Raouf, A., Hassanizadeh, S.M., Leijnse, A., 2010. Upscaling transport of adsorbing solutes in porous media: Pore-network modeling. *Vadose Zone J.* 9:624–636. <http://dx.doi.org/10.2136/vzj2010.0026>.
- Raouf, A., Nick, H.M., Hassanizadeh, S.M., Spiers, C.J., 2013. PoreFlow: a complex pore-network model for simulation of reactive transport in variably saturated porous media. *Comput. Geosci.* 61:160–174. <http://dx.doi.org/10.1016/j.cageo.2013.08.005>.
- Ren, J., Packman, A.I., Welty, C., 2001. Analysis of an observed relationship between colloid collision efficiency and mean collector grain size. *Colloids Surf. A Physicochem. Eng. Asp.* 191:133–144. [http://dx.doi.org/10.1016/S0927-7757\(01\)00770-1](http://dx.doi.org/10.1016/S0927-7757(01)00770-1).
- Sadeghi, G., Schijven, J.F., Behrends, T., Hassanizadeh, S.M., Gerritse, J., Kleingeld, P.J., 2011. Systematic study of effects of pH and ionic strength on attachment of phage PRD1. *Ground Water* 49 (1):12–19. <http://dx.doi.org/10.1111/j.1745-6584.2010.00767.x>.
- Sasidharan, S., Torkzaban, S., Bradford, S.A., Dillon, P.J., Cook, P.G., 2014. Coupled effects of hydrodynamic and solution chemistry on long-term nanoparticle transport and deposition in saturated porous media. *Colloids Surf. A Physicochem. Eng. Asp.* 457: 169–179. <http://dx.doi.org/10.1016/j.colsurfa.2014.05.075>.
- Schijven, J.F., Simunek, J., 2002. Kinetic modeling of virus transport at the field scale. *J. Contam. Hydrol.* 55, 113–135.
- Seetha, N., Hassanizadeh, S.M., Mohan Kumar, M.S., Raouf, A., 2015a. Correlation equations for average deposition rate coefficients of nanoparticles in a cylindrical pore. *Water Resour. Res.* 51:8034–8059. <http://dx.doi.org/10.1002/2015WR017723>.
- Seetha, N., Mohan Kumar, M.S., Hassanizadeh, S.M., 2015b. Modeling the co-transport of viruses and colloids in unsaturated porous media. *J. Contam. Hydrol.* 181:82–101. <http://dx.doi.org/10.1016/j.jconhyd.2015.01.002>.
- Shani, C., Weisbrod, N., Yakirevich, A., 2008. Colloid transport through saturated sand columns: influence of physical and chemical surface properties on deposition. *Colloids Surf. A Physicochem. Eng. Asp.* 316:142–150. <http://dx.doi.org/10.1016/j.colsurfa.2007.08.047>.
- Sharma, M.M., Yortsos, Y.C., 1987. A network model for deep bed filtration processes. *AIChE J.* 33 (10), 1644–1653.
- Shen, C., Huang, Y., Li, B., Jin, Y., 2008. Effects of solution chemistry on straining of colloids in porous media under unfavorable conditions. *Water Resour. Res.* 44, W05419. <http://dx.doi.org/10.1029/2007WR006580>.
- Shen, C., Huang, Y., Li, B., Jin, Y., 2010. Predicting attachment efficiency of colloid deposition under unfavorable attachment conditions. *Water Resour. Res.* 46, W11526. <http://dx.doi.org/10.1029/2010WR009218>.
- Shen, C., Li, B., Huang, Y., Jin, Y., 2007. Kinetics of coupled primary- and secondary-minimum deposition of colloids under unfavorable chemical conditions. *Environ. Sci. Technol.* 41:6976–6982. <http://dx.doi.org/10.1021/es070210c>.
- Shen, C., Li, B., Wang, C., Huang, Y., Jin, Y., 2011. Surface roughness effect on deposition of nano- and micro-sized colloids in saturated columns at different solution ionic strengths. *Vadose Zone J.* 10, 1071–1081.
- Shen, C., Zhang, M., Zhang, S., Wang, Z., Zhang, H., Li, B., Huang, Y., 2015. Influence of surface heterogeneities on reversibility of fullerene (nC<sub>60</sub>) nanoparticle attachment in saturated porous media. *J. Hazard. Mater.* 290:60–68. <http://dx.doi.org/10.1016/j.jhazmat.2015.02.067>.
- Spielman, L.A., Friedlander, S.K., 1974. Role of the electrical double layer in particle deposition by convective diffusion. *J. Colloid Interface Sci.* 46 (1):22–31. [http://dx.doi.org/10.1016/0021-9797\(74\)90021-6](http://dx.doi.org/10.1016/0021-9797(74)90021-6).
- Suchomel, B.J., Chen, B.M., Allen III, M.B., 1998. Network model of flow, transport and biofilm effects in porous media. *Transp. Porous Media* 30, 1–23.
- Sugita, F., Gillham, R.W., Charles, M., 1995. Pore scale variation in retardation factor as a cause of nonideal reactive breakthrough curves 2. Pore network analysis. *Water Resour. Res.* 31 (1), 113–119.
- Syngouna, V.I., Chrysikopoulos, C.V., 2010. Interaction between viruses and clays in static and dynamic batch systems. *Environ. Sci. Technol.* 44:4539–4544. <http://dx.doi.org/10.1021/es100107a>.
- Syngouna, V.I., Chrysikopoulos, C.V., 2013. Cotransport of clay colloids and viruses in water saturated porous media. *Colloids Surf. A Physicochem. Eng. Asp.* 416:56–65. <http://dx.doi.org/10.1016/j.colsurfa.2012.10.018>.
- Thullner, M., Zeyer, J., Kinzelbach, W., 2002. Influence of microbial growth on hydraulic properties of pore networks. *Transp. Porous Media* 49, 99–122.
- Tong, M., Johnson, W.P., 2006. Excess colloid retention in porous media as a function of colloid size, fluid velocity, and grain angularity. *Environ. Sci. Technol.* 40: 7725–7731. <http://dx.doi.org/10.1021/es061201r>.
- Tong, M., Johnson, W.P., 2007. Colloid population heterogeneity drives hyperexponential deviation from classic filtration theory. *Environ. Sci. Technol.* 41, 493–499.
- Torkzaban, S., Bradford, S.A., 2016. Critical role of surface roughness on colloid retention and release in porous media. *Water Res.* 88, 274–284.
- Tosco, T., Bosch, J., Meckenstock, R.U., Sethi, R., 2012. Transport of ferrihydrite nanoparticles in saturated porous media: role of ionic strength and flow rate. *Environ. Sci. Technol.* 46:4008–4015. <http://dx.doi.org/10.1021/es202643c>.
- Trauscht, J., Pazmino, E., Johnson, W.P., 2015. Prediction of nanoparticle and colloid attachment on unfavorable mineral surfaces using representative discrete heterogeneity. *Langmuir* 31, 9366–9378.
- Tufenkji, N., Elimelech, M., 2004. Correlation equation for predicting single-collector efficiency in physicochemical filtration in saturated porous media. *Environ. Sci. Technol.* 38:529–536. <http://dx.doi.org/10.1021/es034049r>.

- Tufenkji, N., Elimelech, M., 2005. Breakdown of colloid filtration theory: role of the secondary energy minimum and surface charge heterogeneities. *Langmuir* 21: 841–852. <http://dx.doi.org/10.1021/la048102g>.
- Valvatne, P.H., Piri, M., Lopez, X., Blunt, M.J., 2005. Predictive pore-scale modeling of single and multiphase flow. *Transp. Porous Media* 58:23–41. <http://dx.doi.org/10.1007/s11242-004-5468-2>.
- Van Marcke, P., Verleye, B., Carmeliet, J., Roose, D., Swennen, R., 2010. An improved pore network model for the computation of saturated permeability of porous rock. *Transp. Porous Media* 85:451–476. <http://dx.doi.org/10.1007/s11242-010-9572-1>.
- Vasiliadou, I.A., Chrysikopoulos, C.V., 2011. Cotransport of *Pseudomonas putida* and kaolin particles through water-saturated columns packed with glass beads. *Water Resour. Res.* 47, W02543. <http://dx.doi.org/10.1029/2010WR009560>.
- Vasilyev, L., Raouf, A., Nordbotten, J.M., 2012. Effect of mean network coordination number on dispersivity characteristics. *Transp. Porous Media* 95 (2):447–463. <http://dx.doi.org/10.1007/s11242-012-0054-5>.
- Vervoort, R.W., Cattle, S.R., 2003. Linking hydraulic conductivity and tortuosity parameters to pore space geometry and pore-size distribution. *J. Hydrol.* 272, 36–49.
- Verwey, E.J.W., Overbeek, J.T.G., 1948. *Theory of the Stability of Lyophobic Colloids*. Elsevier, Amsterdam, Netherlands.
- Wang, C., Bobba, A.D., Attinti, R., Shen, C., Lazouskaya, V., Wang, L., Jin, Y., 2012. Retention and transport of silica nanoparticles in saturated porous media: effect of concentration and particle size. *Environ. Sci. Technol.* 46:7151–7158. <http://dx.doi.org/10.1021/es300314n>.
- Wood, B.D., Quintard, M., Whitaker, S., 2004. Estimation of adsorption rate coefficients based on the Smoluchowski equation. *Chem. Eng. Sci.* 59:1905–1921. <http://dx.doi.org/10.1016/j.ces.2003.12.021>.
- Yao, K.M., Habibian, M.T., O'Melia, C.R., 1971. Water and waste water filtration: concepts and applications. *Environ. Sci. Technol.* 5 (11):1105–1112. <http://dx.doi.org/10.1021/es60058a005>.
- Zhang, Q., Hassanizadeh, S.M., Karadimitriou, N.K., Raouf, A., Liu, B., Kleingeld, P.J., Imhof, A., 2013. Retention and remobilization of colloids during steady-state and transient two-phase flow. *Water Resour. Res.* 49:8005–8016. <http://dx.doi.org/10.1002/2013WR014345>.
- Zhang, Q., Raouf, A., Hassanizadeh, S.M., 2015. Pore-scale study of flow rate on colloid attachment and remobilization in a saturated micromodel. *J. Environ. Qual.* 44 (5): 1376–1383. <http://dx.doi.org/10.2134/jeq2015.01.0058>.
- Zhuang, J., Qi, J., Jin, Y., 2005. Retention and transport of amphiphilic colloids under unsaturated flow conditions: effect of particle size and surface property. *Environ. Sci. Technol.* 39:7853–7859. <http://dx.doi.org/10.1021/es050265j>.